INVESTIGATION OF AEROBRAKING TO RETURN THE SPACE MANEUVER
VEHICLE TO LOW EARTH ORBIT FROM GEOTRANSFER ORBIT

THESIS

Benjamin M. Berlin, Second Lieutenant, USAF

AFIT/GA/ENY/05-M01

DEPARTMENT OF THE AIR FORCE
AIR UNIVERSITY

AIR FORCE INSTITUTE OF TECHNOLOGY

Wright-Patterson Air Force Base, Ohio

	Form Approved OMB No. 0704-0188

Report Documentation Page

1. REPORT DATE **09 MAR 2005**	2. REPORT TYPE **N/A**	3. DATES COVERED **-**

4. TITLE AND SUBTITLE	5a. CONTRACT NUMBER
Investigation Of Aerobraking To Return The Space Maneuver Vehicle To Low Earth Orbit From Geotransfer Orbit	5b. GRANT NUMBER
	5c. PROGRAM ELEMENT NUMBER
6. AUTHOR(S)	5d. PROJECT NUMBER
	5e. TASK NUMBER
	5f. WORK UNIT NUMBER
7. PERFORMING ORGANIZATION NAME(S) AND ADDRESS(ES) **Air Force Institute of Technology Air University**	8. PERFORMING ORGANIZATION REPORT NUMBER
9. SPONSORING/MONITORING AGENCY NAME(S) AND ADDRESS(ES)	10. SPONSOR/MONITOR'S ACRONYM(S)
	11. SPONSOR/MONITOR'S REPORT NUMBER(S)

12. DISTRIBUTION/AVAILABILITY STATEMENT
Approved for public release, distribution unlimited

13. SUPPLEMENTARY NOTES
The original document contains color images.

14. ABSTRACT

15. SUBJECT TERMS

16. SECURITY CLASSIFICATION OF:			17. LIMITATION OF ABSTRACT **UU**	18. NUMBER OF PAGES **116**	19a. NAME OF RESPONSIBLE PERSON
a. REPORT **unclassified**	b. ABSTRACT **unclassified**	c. THIS PAGE **unclassified**			

Standard Form 298 (Rev. 8-98)
Prescribed by ANSI Std Z39-18

AFIT/GA/ENY/05-M01

Investigation Of Aerobraking To Return The Space Maneuver Vehicle To Low Earth Orbit From Geotransfer Orbit

THESIS

Presented to the Faculty

Department of Aeronautics and Astronautics

Graduate School of Engineering and Management

Air Force Institute of Technology

Air University

Air Education and Training Command

In Partial Fulfillment of the Requirements for the

Degree of Master of Science in Astronautical Engineering

Benjamin M. Berlin, B.S.

Second Lieutenant, USAF

March, 2005

AFIT/GA/ENY/05-M01

Investigation Of Aerobraking To Return The Space Maneuver Vehicle To Low Earth Orbit From Geotransfer Orbit

Benjamin M. Berlin, B.S.

Second Lieutenant, USAF

Approved:

/signed/	9 Mar 2005
Dr. William E. Wiesel (Chairman)	date
/signed/	9 Mar 2005
LtCol Kerry D. Hicks (Member)	date
/signed/	9 Mar 2005
LtCol Nathan A. Titus (Member)	date

AFIT/GA/ENY/05-M01

Abstract

This study investigated the use of ballistic and "Double-Dip" aerobraking reentry to return the Space Maneuver Vehicle (SMV) from geotransfer orbit in no more than two atmosphere passes. Lift and drag accelerations were applied to the two-body problem when either of their magnitudes exceeded $\frac{1}{1000}$ g. Lift and drag coefficients, along with the SMV model, were taken from *Investigation of Atmospheric Reentry for the Space Maneuver Vehicle* by Captain McNabb, AFIT/GA/ENY/04-M03. Target perigees were formulated using the two-body problem. The orbit from each target perigee was numerically integrated around a planar earth model using a fourth order Runge-Kutta method. Ballistic and "Double-Dip" reentry schemes were attempted with 45 and 70 km altitude floors. Ballistic reentry produced a near circular, low earth orbit when the SMV's perigee altitude resided between 66.801 and 68.449 km for a one pass reentry and 72.226 and 73.445 km for a two pass reentry. "Double-Dip" reentry produced a near circular, low earth orbit when the SMV's perigee altitude rested between 62.416 and 64.962 km. The resulting perigee windows, their respective heating rates, and experienced accelerations were analyzed. Effects of uncertainty in the atmosphere model on successful perigee windows for each reentry scheme were analyzed by repeating the simulation with an increased atmospheric density.

Acknowledgements

Table of Contents

List of Figures

ix

xi

List of Tables

Investigation Of Aerobraking To Return The Space Maneuver Vehicle To Low Earth Orbit From Geotransfer Orbit

I. Introduction

Background

The 1999 Department of Defense Space Policy states,

> Space is a medium like the land, sea, and air within which military activities will be conducted to achieve U.S. national security objectives. The ability to access and utilize space is a vital national interest because many of the activities conducted in the medium are critical to U.S. national security and economic well-being. The globally interdependent information- and knowledge-based economy as well as information-based military operations make the information lines of communication to, in, through, and from space essential to the exercise of U.S. power. [3, 2]

The United States' need to effectively control space and effectively defend its space assets increases every day. Not only have our war fighters become exceedingly dependent on satellites for top-of-the-line battlefield awareness and communication, U.S. fighters and bombers also rely on the Global Positioning System (GPS) constellation to guide their smart bombs, and many of the U.S. intelligence services rely on satellite imagery to investigate the actions of countries deep within their borders. When a satellite breaks, launching a new payload into space can take years following the current space launch paradigm, but if the U.S. is to effectively defend its space superiority, a quick launch vehicle must be developed. Air Force Space Command has suggested developing the Military Space Plane (MSP) in order to fill this need. The MSP has four primary components [13, 1-2]:

- Space Operations Vehicle (SOV): a reusable launch element to reduce the cost of, improve the flexibility of, and increase the responsiveness of earth-to-orbit operations;

- Space Maneuver Vehicle (SMV): an uncrewed, reusable satellite bus and upper stage with significant maneuvering capability;

- Modular Insertion Stage (MIS): a low cost expendable upper stage to reduce the cost and improve the operability of Space Support missions;

- Common Aero Vehicle (CAV): an aeroshell designed to deliver material (e.g. munitions, UAVs, or critical supplies) through space directly to a theater.

"The military needs reliable, responsive, cost-effective, and assured access to space" [14, 1]. The SMV is of primary concern in this study because it fulfills the military's need stated above. "The SMV system concept combines the best of aircraft and space elements into a low cost, low risk package which specifically addresses multiple warfighter needs. With this capability, the SMV can provide the United States with a flexible space superiority capability sufficient to maintain battlefield dominance in support of future warfighter operations" [10, 2]. An operational SMV might include [1]:

- Up to 1,200 pounds of sensors/payload

- 72-hours or less turnaround time between missions

- Up to 12-month, on-orbit mission duration

- Rapid recall from orbit

- Up to 3.2 km/s on-orbit velocity change for maneuvering

Protecting and repairing friendly assets, identifying and destroying space threats, and placing new satellites into orbit are the five most important pillars to truly commanding control of space. According to AFRL the SMV could perform missions such as [1]:

- Intelligence, surveillance and reconnaissance of ground targets (with either integrated or deployable ISR satellite)

- Deployment and recovery of microsatellites (e.g. Space Control Satellites)

- Rapid constellation replenishment

Past Research

There have been several spacecraft and concepts developed that have furthered the technology needed to field the SMV. In 2001, the National Aeronautics and Space Administration (NASA) withdrew funding from the X-33, a single stage to orbit vehicle, and the X-34, a reusable, unmanned suborbital spacecraft [4]. The X-34 flight test model, built by Orbital Sciences Corporation, was 58.3 feet long, had a wingspan of 57.7 feet, and stood 11.5 feet tall. It was to be powered by a reusable Fastrac engine, an engine that provides 60,000 pounds of thrust and is aimed at boosting payloads up to 500 pounds [17]. The X-34 was designed "to be air-launched from Orbital Science's L-1011 aircraft, then accelerated to speeds up to Mach 8, reaching altitudes up to 250,000 feet. It was to land horizontally on a conventional runway" [8]. Figure 1 shows the X-34.

Figure 1:   X-34 [17]

The X-33 was envisioned to be 69 feet long and have a wingspan of 77 feet. Two J-2S Linear Aerospike engines were to provide 410,000 pounds of thrust to lift the 285,000-pound vehicle to low earth orbit. The X-33 was to launch vertically like a rocket, reaching a suborbital altitude at speeds greater than Mach 13, and then land like an airplane [18]. The X-33 was supposed to be a testbed for a reusable cryogenic

tank system, cryogenic insulation, and an integrated thermal protection system [7]. It was also going to verify the thermal protection system durability, demonstrate guidance, navigation, and control systems including autonomous flight control during takeoff, ascent, flight, reentry, and landing [7]. Figure 2 shows an artist's conception of the X-33.

Figure 2:   Artist's Conception of X-33 [18]

Although the X-33 and X-34 programs ended in 2001, two new programs, the X-40A and X-37, made and are making gigantic leaps forward in automated spacecraft technology. The X-40A is an eighty-five percent scale model of the X-37 that completed its seventh and final automated landing test on 17 May 2001 [6]. The X-40A, shown in Figure 3, successfully validated the low speed atmospheric flight dynamics of the X-37 at NASA Dryden Research Center after it was dropped seven times from an Army Chinook helicopter, acquired the runway, and performed a successful landing [6].

The X-37, shown in Figure 4, is being assembled by Boeing at their High Desert Assembly, Integration and Test Facility in Palmdale, California [5]. "The re-usable space plane will demonstrate 41 airframe, propulsion and operations technologies aimed at significantly cutting the cost of space flight. The X-37 can be carried into orbit by the Space Shuttle or be launched by an expendable rocket" [21].

Richard Powell led a study for NASA in 1985 concerning an aerobraking procedure to return a spacecraft from geosynchronous orbit to low earth orbit in order

NASA Dryden Flight Research Center Photo Collection
http://www.dfrc.nasa.gov/gallery/photo/index.html
NASA Photo: EC01-0148-4   Date: May 8, 2001   Photo by: Jim Ross

X-40A Free Flight #5

Figure 3:   X-40A [6]

NASA Dryden Flight Research Center Photo Collection
http://www.dfrc.nasa.gov/Gallery/Photo/index.html
NASA Photo: EC99–45145–2   Date: 1999

Illustration of the X–37 Advanced Technology Demonstrator during flight

Figure 4:   X-37 [16]

to rendezvous with the Space Shuttle. The Aero-assisted Orbital Transfer Vehicle (AOTV) was designed to leave geosynchronous orbit by performing a small burn to lower its perigee into the atmosphere. After aerobraking during its first dip into the

atmosphere, the AOTV would enter a 300 nautical mile phasing orbit where it would perform a second burn to lower itself into the Space Shuttle's orbit. It would circularize its orbit with a third burn and rendezvous with the Space Shuttle [15, 46]. Figure 5 shows the conceptual high lift-to-drag AOTV, and Figure 6 shows the AOTV's envisioned mission profile.
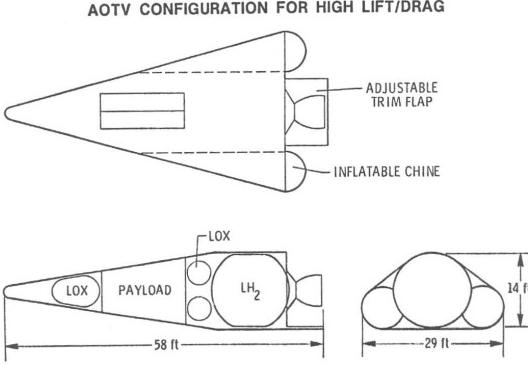
Figure 5:   AOTV Configuration for High Lift/Drag [15, 44]
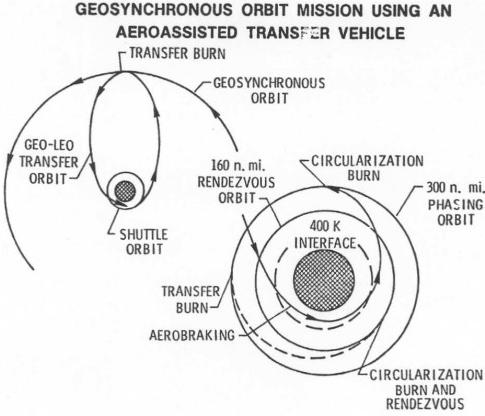
Figure 6:   Potential AOTV Aerobreaking Flight Path [15, 46]

The NASA study led by Powell lends a great deal of plausibility to this study's search for an aerobraking orbit that returns the SMV to a low earth orbit. The aerodynamic performance charts reveal that the SMV and AOTV share similar characteristics [15, 45]. At a perigee of 70 kilometers, the SMV has a coefficient of lift of approximately 0.51, a lift-to-drag ratio around .807, and travels at roughly 93 percent of escape speed. Comparing the SMV's traits to the AOTV's traits reveals that the

6

AOTV and SMV are not identical but are very similar. Figure 7 shows the AOTV's aerodynamic properties.
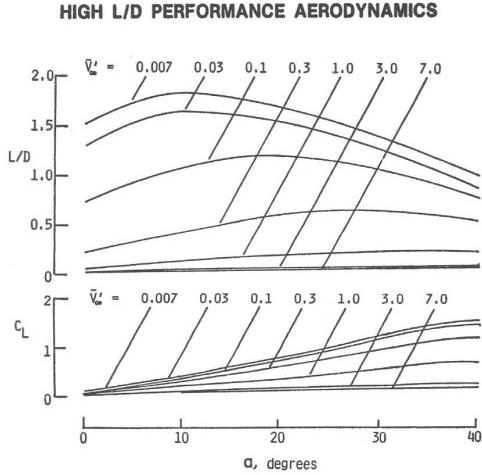
Figure 7:   High L/D AOTV Performance Aerodynamics [15, 45]

The AOTV's altitude history will be used to help determine what altitude to start the simulation. While the AOTV was aerobraking it dipped to an altitude near 54.8 kilometers [15, 47] as seen in Figure 8. This study will begin at 45 kilometers and gradually increase the SMV's perigee altitude. There was a difference in Powell's study that might affect the outcome of this two dimensional study. Powell's simulation was three dimensional and accounted for any inclination change required to rendezvous with the shuttle. The extra energy bled off during an inclination change in the Powell study, but not accounted for in this study, might lead to failure.

A large amount of information is drawn from Captain Dennis McNabb's thesis, ENY/04-M03, entitled *Investigation of Atmospheric Reentry for the Space Maneuver Vehicle.* His results will be discussed in Chapter II.

Concept of Operations

The current space launch paradigm prohibits swift launch or retrieval missions. The inability to quickly repair or replace friendly spacecraft and assess or destroy unfriendly spacecraft severely limits the Department of Defense's ability to protect

7
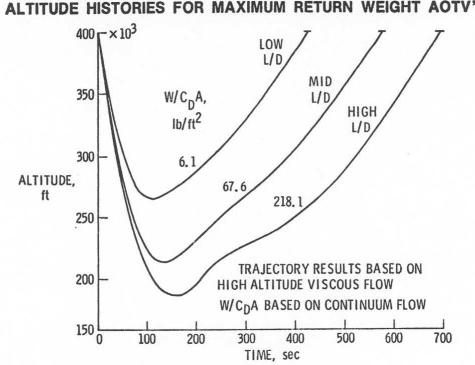
Figure 8: Altitude History for Maximum Return Weight AOTV [15, 47]

the United States. Without guaranteed space access, troops in the field might lose realtime communications, and hostile activities might go undetected. Analysis of the SMV's proposed capabilities will reveal that the SMV would fill that gap.

The SMV will be delivered to a circular, low earth orbit by either an Evolved Expendable Launch Vehicle (EELV) or one of the space shuttles. Equation 1 gives the required ΔV for a coplanar burn from a circular, low earth orbit to geotransfer orbit [22, 305-306].

$$\Delta V = \sqrt{2\frac{\mu}{r} + \varepsilon} - \sqrt{\frac{\mu}{r}} \qquad (1)$$

where

$\mu = 398600.5 \ (km^3/s^2)$

r = Magnitude of SMV position vector (km)

ε = Energy of transfer orbit

From a 400 km circular orbit, a ΔV of approximately 2.4 km/s is required to enter geotransfer orbit. Assuming an instantaneous burn, the Hohmann transfer orbit would deliver the SMV to the target position or satellite in slightly under 5.3 hours. After it arrives at its target the SMV could perform any number of tasks. Once its task was accomplished, the SMV would be faced with the difficult task of returning to earth for any necessary changes or repairs. The SMV's advertised ΔV capability of 3.2 km/s is 1.6 km/s short of the 4.8 km/s required for a two burn round trip. If

8

the SMV is going to operate in geotransfer orbits, an alternate return method must be developed. Aerobraking, the process of dipping a spacecraft's perigee into the atmosphere in order to retard its velocity and shorten its semimajor axis, will allow the SMV to undertake geotransfer missions and make it back with enough fuel to reenter and land. In order to aerobrake, the SMV would need to perform a small burn at apogee, $\Delta V = 0.038$ km/s, in order to dip its perigee into the atmosphere. Once the SMV finished its aerobraking maneuver, it would, if needed, perform a small burn to raise its perigee above any noticeable atmospheric effects. After completing the aerobrake maneuver and circularization burn, it would be in a near circular, low earth, phasing orbit. The SMV could proceed directly from its phasing orbit into a reentry-to-land flight profile or could orbit the earth several times before reentering in order to minimize the required maneuvering in the continuum flight regime.

Research Objectives

The purpose of this study is to explore the possibility that the SMV can fly out to a target in geosynchronous orbit, perform a set of preprogrammed tasks on its target, and return to a circular, low earth orbit in no more than two orbits by aerobraking. This simulation assumes that the SMV has travelled to its target, successfully completed its task, and now needs to return to low earth orbit. Aerobraking
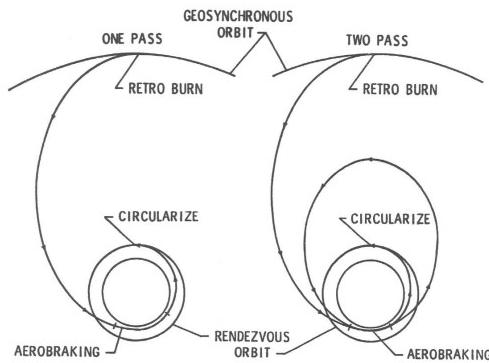
Figure 9:   One and two-pass aerobraking orbits [15, 55]

will allow the SMV to expend a majority of its fuel on the outbound trip instead

9

of having to save a great deal of it for the return trip and landing procedure. This greatly enhances its operational capabilities and makes finding a viable orbit trajectory of the utmost importance. Figure 9 depicts two potential aerobraking orbits. There are many possible aerobraking schemes, but this study will focus on two, ballistic entry and the "Double-Dip" reentry method described in Chapter Eight of Wiesel's *Spaceflight Dynamics*. This study hopes to find the window of perigee altitudes that allows the SMV to maneuver from geotransfer orbit to a low earth circular orbit in no more than two passes using both reentry algorithms.

Chapter II will deal extensively with the problem setup. It begins by explaining the simulation's atmosphere model, its planar earth assumption, the SMV model, the SMV's aerodynamic properties, and the mechanics of the simulation's numerical integrator. The development of the equations of motion for both reentry schemes follows the discussion of the assumptions. Chapter II concludes with a detailed explanation of the "Double-Dip" reentry.

Chapter III delves into the mechanics of the simulation. It begins by explaining how the simulation's initial and final conditions were determined. It will also detail the algorithm used to build the computer simulation. Chapter III ends with discussion of each subroutine.

Chapter IV will detail the simulation's results. It begins by discussing the determination of the bifurcation point using both ballistic entry and "Double-Dip" reentry. It will then discuss the successful perigee altitude choices, disregarding any constraints, for the ballistic entry. Potential "Double-Dip" solutions will be reviewed. Immediately following the "Double-Dip" solution discussion, the required technological advancements for both solutions to work will be discussed. Plots of the experience accelerations and the heating rate will be shown to display any SMV shortcomings. Plots of the SMV's flight path, velocity, and altitude will be given in order to verify successful mission completion. Chapter IV will end with successful perigee window atmospheric sensitivity analysis.

Chapter V will summarize the results of applying a ballistic and "Double-Dip" reentry scheme to the SMV's return to low earth orbit. The results are interpreted to display the need for an active control system on board any vehicle performing an aerobraking maneuver with a short allowed mission completion time. Chapter V ends by noting areas of model improvement and future areas of study.

II. Problem Setup

Chapter Overview

Chapter II starts by discussing the physical assumptions made to simplify the problem and goes on to discuss the SMV's aerodynamic characteristics. After establishing the framework for a simulation, the simulation's numerical integrator is identified and discussed. It is immediately followed by the development of the equations of motion. Finally, the details of ballistic and "Double-Dip" reentry are discussed.

Physical Assumptions

It is important to establish and justify the simulation's assumptions concerning the atmosphere, earth's geometry, aerodynamic forces, and SMV characteristics before constructing the model because they greatly impact the performance and accuracy of the model. While this thesis is a proof-of-concept simulation and does not need to include every minute perturbation, future models used to validate operational capabilities would be wise to include third-body gravitational forces, solar wind pressure, the nonspherical earth gravitational accelerations, and any vehicle thrust. These perturbations are extremely small, but they would need to be added to the simulation in an application that requires a high degree of accuracy.

Atmospheric Assumptions.   This simulation depends on the interaction between lift and drag to place the SMV in a low earth circular orbit. Nothing is more important in determining lift and drag than atmospheric density, and nothing could be more difficult to accurately discern. The atmosphere is highly volatile, and the density at any location is affected by latitudinal and longitudinal variations, fluctuations in solar activity, magnetic storms, and ocean tides, etc. [22, 524-526]. The simulation was run with a combined Vallado and Regan atmosphere. To highlight the need for an active control system on this mission because of atmospheric fluctuations, any successful orbits were integrated again assuming a five percent increase in atmospheric density. The sensitivity analysis will be discussed in Chapter IV.

The simulation uses a combination of the layered exponential atmosphere described by Vallado and the exponential atmosphere described by Regan and Anandakrishnan. It uses Regan's and Anandakrishnan's model below 120 km and Vallado's above 120 km. Below 120 kilometers [20, 38]

$$\rho = \rho_0 \, e^{-h/H} \tag{2}$$

where

ρ_0 = Sea level density $(1.752 \; kg/m^3)$

h = SMV altitude at any time below 120 km (km)

H = Scale Height $(6.7 \text{ x } 10^3 \; m)$

At altitudes above 120 km, Vallado's model breaks the atmosphere into smaller layers, each with a unique nominal density and scale height. Above 120 km, the atmospheric density is found by using the following equation as a model for each altitude layer [22, 532-534]:

$$\rho = \rho_0 * exp(-\frac{h_{ellp} - h_0}{H}) \tag{3}$$

where

ρ = Atmospheric density at altitude (kg/km^3)

ρ_0 = Reference density at h_0 (kg/km^3)

h_0 = Reference altitude (km)

h_{ellp} = Height above the ellipsoid (km)

H = Scale height at altitude layer (km)

Regan's atmosphere model closely matches the 1976 U. S. Standard Atmosphere up to 120 km [20, 39]. Vallado's model atmosphere derives its values from 25-500 km from CIRA-72 and uses CIRA-72 with exospheric temperature, $T_\infty = 1000 \; K$ for

500-1000 km [22, 534]. Figure 10 shows the atmospheric density at altitudes from 0-1000 km using the combined model.
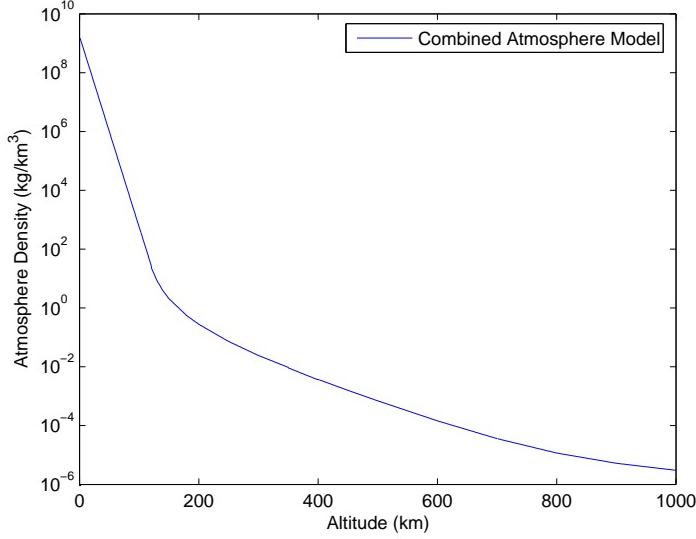
Figure 10:   Atmospheric Density Versus Altitude [22, 532-534]

The Matlab code used for the simulation's combined atmosphere model can be found on the compact disc that accompanies this thesis. It is also assumed that the atmosphere's velocity at any given point is parallel to that location's latitude and does not act in the radial direction.

Earth Geometry.   The earth is not a perfect sphere, but the perturbing accelerations due to a nonspherical earth are negligible compared to the lift, drag, and gravity forces over the period of one or two orbits. Because the SMV's return from geotransfer orbit will only span one or, at most, two orbits, the earth is modeled as a sphere with evenly distributed mass. Future operational models will have to account for these accelerations.

The SMV's geotransfer orbit can intersect its target at any inclination, and because perturbing forces are constrained to the orbit plane, the SMV's inclination, while not necessarily zero, can be ignored. The spherical earth assumption allows a further simplification to a two dimensional, circular earth. This assumption is valid as

long as the lift vector acts only in the position-velocity plane. Conveniently enough, this simulation constrains the lift vector to the position-velocity plane.

Aerodynamic Forces. The question, "When should atmospheric perturbations be considered?" is difficult to answer because the addition of aerodynamic forces increases the simulation run time due to the increasingly complex acceleration components input into the numerical integrator. However, in later discussion about the "Double-Dip" reentry scenario, atmospheric entry must be considered well above any noticeable accelerations. In order to maintain validity, lift and drag are considered when either of their magnitudes are greater than 0.001g. This assumption causes the simulation to begin considering lift and drag near 130 km. The off-on "light switch" method reduces the numerical integration to the two-body problem when lift and drag are negligible.

As will be seen below, the SMV's aerodynamic characteristics differ in each of the three flowfields: continuum flow, transition flow, and free molecular flow. These flowfields are defined by describing the relaxation time and distance for their constituent molecules [20, 314]. A flowfield with a high number of molecules has a high intermolecular collision frequency and short relaxation distance and time [20, 313]. "If this relaxation distance is small compared to the characteristic dimension of the flowfield, the macroscopic properties can be considered continuously" [20, 313]. Free molecular flow has relaxation distances greater than the characteristic flowfield dimension [20, 314]. In this condition, the state of individual molecules must be considered. Thus, Newtonian impact theory is the governing equation for this flowfield [20, 314]. A nondimensional parameter, called the Knudsen number, was created to help differentiate between the flowfields [20, 314]. The Knudsen number is equal to [20, 314]

$$Kn = \frac{\lambda}{L} = \frac{mean\ free\ path}{characteristic\ flowfield\ dimension} \qquad (4)$$

It is widely held that Knudsen numbers $>> 1$ describe free molecular flow, and Knudsen numbers $<< 1$ pertain to continuum [20, 316]. As in Captain McNabb's study, "regions where Kn > 10 will be considered free molecular flow" [13, 15], and "the region where Kn $< .01$, the flowfield will be treated as continuum flow" [13, 15]. Transition flow resides between continuum and free molecular flow. The SMV will traverse all three regimes as it dips into the atmosphere. Captain McNabb supplied equations for C_L and C_D in molecular free flow and continuum. In order not to over complicate this simple model, values for C_L and C_D in transition flow were determined by linearly interpolating between the molecular free flow and continuum values. Figure 11 presents a graph of altitude versus Knudsen number.
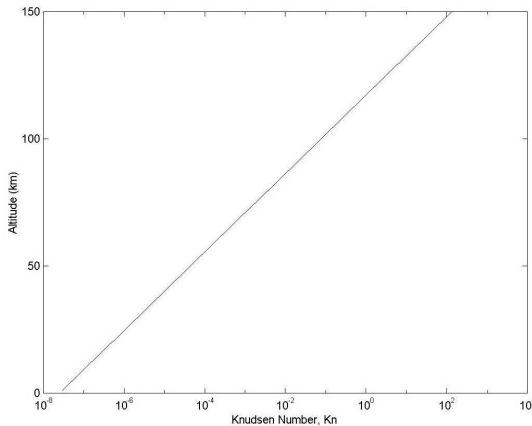
Figure 11:   Altitude Versus Knudsen Number [13, 16]

SMV Characteristics

In his thesis, Captain Dennis McNabb dutifully acknowledged the fact that the SMV does not exist. This fact sent him searching for potential flight vehicle models. He struck engineering gold and found Boeing SMV concept data and Boeing X-37 concept drawings [13, 11].

Captain McNabb used concept drawings of the Boeing X-37 to deduce its body width, nose width, and chord length [13, 12]. He then used these figures to build a 60-panel model of the SMV. Appendix B shows Captain McNabb's 60-panel model. This

Table 1:   Conceptual SMV Parameters [13, 12]

Parameter	Value
Weight	44482.216 N
Length	8.8392 m
Wingspan	4.572 m
Height	2.8956 m
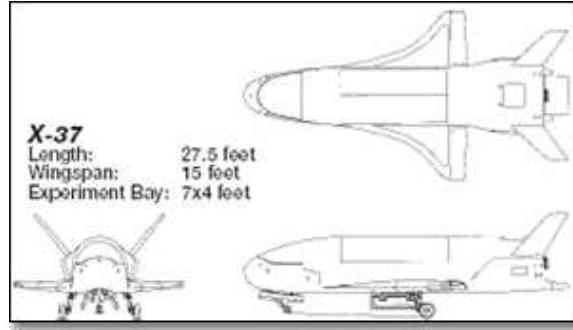
Figure 12:   Boeing X-37 [13, 12]

model was used to determine the SMV's lift and drag coefficients at varying angles of attack and flow field conditions. He performed a quadratic regression from fifteen to fifty degrees angle of attack to find equations for the lift and drag coefficients. Appendix C contains graphs of his best fit lines. His equations for the lift and drag coefficients in free molecular flow and continuum are given below [13, 20-22]:

$$C_{LC} = -3.3069 * 10^{-4}(AOA)^2 + 0.0552 * (AOA) - 0.5034 \tag{5}$$

$$C_{LF} = -3.8241 * 10^{-5} * (AOA)^2 + 0.0033 * (AOA) - 0.0022 \tag{6}$$

$$C_{DC} = 9.6602 * 10^{-4} * (AOA)^2 - 0.0150 * (AOA) + 0.2402 \tag{7}$$

$$C_{DF} = -1.3241 * 10^{-4} * (AOA)^2 + 0.0373 * (AOA) + 0.2265 \tag{8}$$

where

C_{LC} = Coefficient of lift in continuum

C_{LF} = Coefficient of lift in free flow

C_{DC} = Coefficient of drag in continuum

C_{DF} = Coefficient of drag in free flow

The ballistic simulation used a $C_{DF} = 2.0$ and a $C_{DC} = 3.75$ in continuum. A linear interpolation supplied C_D values for the transition region. C_{LC} and $C_{LF} = 0$ for the ballistic reentry. The "Double-Dip" reentry simulation was run twice using the SMV's best C_L/C_D angle of attack, 21°, and twice at the maximum C_D in Captain McNabb's angle of attack window, 50° [13, 22-23]. Appendix C displays the lift and drag coefficients computed from McNabb's equations and their ratios.

Runge-Kutta Method of Fourth Order

The Runge-Kutta Method of Fourth Order refers to numerical integration methods "originally presented by Carl Runge (1856-1927) in 1895, and Wilhelm Kutta (1867-1944) in 1901, which also derive from a Taylor series" [22, 500]. The Runge-Kutta Method is a single-step numerical integrator; this means it "combines the state at one time with rates at several other times, based on the single-state value at time, t_0" [22, 499]. It calculates those rates at four different locations in each time interval using a fourth-order Taylor series expansion [22, 500]. "The rates are readily obtained from the equations of motion and allow us to determine the state at succeeding times, $t_0 + h$" [22, 499]. Before the Runge-Kutta equations are given, the state vector must be defined.

$$X = \begin{bmatrix} \vec{r} \\ \vec{v} \end{bmatrix} \qquad (9)$$

where

$\vec{r}$ = SMV inertial position vector

$\vec{v}$ = SMV inertial velocity vector

Taking the state vector's derivative with respect to time yields

$$\dot{X} = \begin{bmatrix} \vec{v} \\ \vec{a} \end{bmatrix} \tag{10}$$

where

$\vec{a}$ = SMV inertial acceleration vector

Vallado defines the function $\bar{f}(t, y) = \dot{X} = \dot{y}(t)$ [22, 500]. The Runge-Kutta integrator will calculate the values of $\dot{X}$ using the following equations [22, 500]:

$$
\begin{aligned}
\dot{y}_1 &= f(t_0, y_0) \\
\dot{y}_2 &= f(t_0 + \frac{h}{2}, y_0 + \frac{h}{2}\dot{y}_1) \\
\dot{y}_3 &= f(t_0 + \frac{h}{2}, y_0 + \frac{h}{2}\dot{y}_2) \\
\dot{y}_4 &= f(t_0 + h, y_0 + h\dot{y}_3) \\
y(t) &= y(t_0) + \frac{h}{6}(\dot{y}_1 + 2\dot{y}_2 + 2\dot{y}_3 + \dot{y}_4) + O(h^5)
\end{aligned} \tag{11}
$$

where

h = Time step (s)

$O(h^5)$ = Error term on the order of h^5

It is immediately obvious that time step selection is vital to producing legitimate results. A test orbit without perturbations was run from apogee to apogee through the Runge-Kutta code to determine the most appropriate value for the simulation's time step. Table 2 shows the errors associated with integrating a two-body orbit for one orbit with five different time steps.

A time step of 1 second was chosen because it was the largest time step to produce less than 0.5 m of error. Time steps larger than 1 s could place the SMV in the wrong atmosphere layer over two orbits and produce erroneous data. The error

Table 2:   Change in Position and Velocity After One Orbit at Differing Time Steps

Time step	0.25s	0.5s	1s	2s	5s
Δ X	.00002 km	.00010 km	.00015 km	.00052 km	.00936 km
Δ Y	.00006 km	.00010 km	.00018 km	.00033 km	.00145 km
$\Delta \dot{X}$	.00009 km/s	.00014 km/s	.00025 km/s	.00048 km/s	.00014 km/s

associated with a 1 s time step is on the same order as a 0.5 s time step. Running the simulation with a time step smaller than 1 s would lengthen run time and, considering the simulation's assumptions, not necessarily produce better results. The effects of adding perturbations on the time step choice must also be considered. Adding perturbations to the model will increase the model's error because the perturbations cause the SMV's accelerations to change rapidly. However, the errors in the SMV's position after one orbit can only be judged relative to its final position using a smaller time step because the SMV's true position and velocity after one orbit can never be known. Therefore, position and velocity errors for a perturbed orbit were not considered in the time step selection. Table 2 does not show the velocity error in the $\hat{e}_y$ direction because it is smaller than 0.5 mm for all of the time steps.

Examination of Equation 11 reveals that the SMV's acceleration vector or equations of motion must be determined before the simulation can begin. This will be accomplished in the next section.

Equations of Motion

There are many different ways to formulate the equations of motion for the SMV, and, due to the simulation's planar earth assumption and the computing power of modern personal computers, the equations are formulated using Cartesian coordinates in the geocentric-equatorial coordinate frame. Hicks describes this coordinate frame:

> The geocentric-equatorial system is an inertial reference frame with its origin at the center of the planet. The x-axis points in the direction of the vernal equinox and the z-axis passes out the north pole. The y-axis completes the system such that it lies in the planet's equatorial plane and $\hat{e}_z = \hat{e}_x \times \hat{e}_y$. [9]

This coordinate frame, while not truly stationary, is suitable enough to be considered inertial. The SMV is constrained to the X-Y plane in the current simulation by cleverly picking its starting position and velocity vectors, but the simulation has the ability to upgrade to handle position, velocity, and acceleration components in the $\hat{e}_z$ direction by retaining zeros in that position that can later be changed.

Newton's second law for fixed mass sytems will be used to find the SMV's inertial acceleration. It states, "The change of motion is proportional to the motive force impressed and is made in the direction of the right line in which that force is impressed" [2, 3]. Newton was simply saying that the force on an object is equal to the time rate change of its momentum, or

$$\vec{F} = \frac{d}{dt}\vec{p} \tag{12}$$

Because the simulation is a fixed mass system, Newton's second law can be simplified into the more recognizable

$$\vec{F} = m\vec{a} \tag{13}$$

where

m = SMV mass (kg)

Finding the SMV's acceleration vector now becomes a matter of describing the forces acting on the SMV and dividing by the mass. The ballistic reentry simulation will consider gravity and drag, while the "Double-Dip" reentry will consider gravity, drag, and lift.

Gravity. Newton recognized that any two masses act on each other with a force "proportional to the product of their masses and inversely proportional to the square of the distance between them" [22, 135]. The earth's mass acts on the SMV

21

along the SMV's inertial position vector with a force that be described by [22, 135]

$$\vec{F}_g = -\frac{Gm_\oplus m_{sat}}{r^2}\frac{\vec{r}}{|\vec{r}|} \tag{14}$$

where

$\vec{F}_g = $ Force of gravity (N)

$G = 6.673 \times 10^{-20} \pm 0.001 \times 10^{-20}\ (km^3 \cdot kg^{-1} \cdot s^{-2})$

$m_\oplus = 5.9733320 \times 10^{24}\ (kg)$

G and $m_\oplus$ are often combined to form the gravitational parameter, μ, because it is easier to measure the gravitational force from the earth felt by a satellite than to accurately measure the mass of the earth and the gravitational attraction between small objects [22, 136]. The simulation's computer code calculates the SMV's gravitational acceleration with the following equation:

$$\vec{a} = -\frac{\mu}{r^2}\frac{\vec{r}}{|\vec{r}|} \tag{15}$$

The simulation was run taking only the effects of gravity on the SMV into account to verify its construction. The SMV's orbit should be one complete ellipse. Figure 13 validates the gravity model.

Lift. Lift plays a leading role in the "Double-Dip" reentry scheme. The SMV enters the earth's atmosphere with its lift vector pointed away from the earth, and as it begins to pull out of the atmosphere, its lift vector is rolled to point towards the earth. This roll maneuver is usually accomplished at a pre-determined flight path angle. There are multiple ways to pick the flight path angle at which the SMV will accomplish its "instantaneous" roll; these will be discussed later in the chapter. In keeping with earlier assumptions, the SMV's lift vector is constrained to the orbit

22
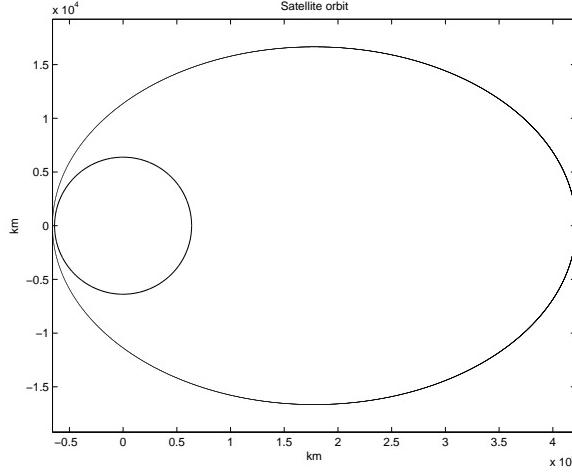
Figure 13: Two-body Orbit

plane. The resulting simplified planar lift is described by the equation [23, 240]:

$$L = \frac{1}{2} * C_L * A * \rho * V_{rel}^2 \tag{16}$$

where

C_L = Coefficient of lift

A = Reference area (km^2)

V_{rel} = SMV velocity relative to the atmosphere (km/s)

The force due to lift is converted into an acceleration by dividing by the SMV's mass. The acceleration due to lift can be expressed by the equation:

$$A_L = \frac{1}{2} * \frac{C_L * A}{m} * \rho * V_{rel}^2 \tag{17}$$

The reference area, or effective lifting surface, was determined from Captain McNabb's MATLAB SMV model. Only the SMV's wings were considered in computing the effective lifting surface, but future studies should consider including the wetted area of the SMV's body that contributes to lift production. The forward lifting surfaces were broken into a rectangle and triangle to more accurately determine their area.

23

The two lifting surfaces had a combined area of approximately $3.875\,m^2$. This lifting surface area was used for the 21° angle of attack case and the 50° angle of attack case. Appendix B contains pictures of Captain McNabb's MATLAB SMV model.

The effects of a roll maneuver with lift on the SMV's orbit are not entirely intuitive. Only a discussion with Dr. Wiesel validated the lift perturbation model. The lift perturbation rotates the orbit's apogee clockwise towards its original perigee. The lower the SMV dips into the atmosphere, the more pronounced this effect becomes. Figure 14 shows the effects of lift on the SMV's orbit when its perigee dips to 15 km, and its angle of attack is 21°. Figure 15 shows the effects of lift on the SMV's orbit when it has a perigee of 45 km and a 21° angle of attack.
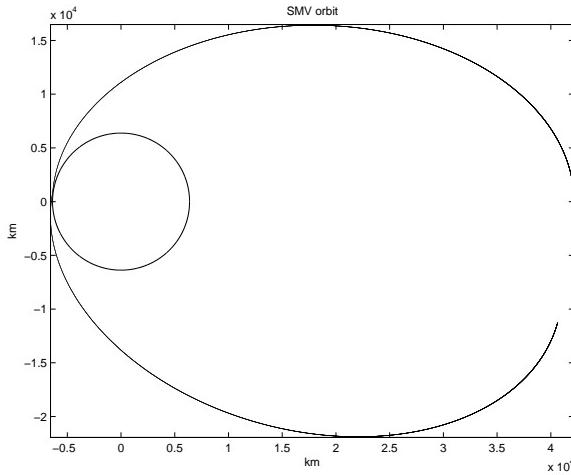
Figure 14:   Lift Perturbed Orbit, Perigee = 15 km

Drag.   The SMV has an enormous amount of kinetic energy as it reenters the atmosphere. The SMV has a total mechanical energy described by [23, 51]:

$$\varepsilon = \frac{1}{2}\nu^2 - \frac{\mu}{r} \tag{18}$$

and a kinetic energy per unit mass T = $v^2/2$ [23]. While it reenters the SMV has a specific energy of roughly -8.2 $(km/s)^2$ and a specific kinetic energy of 50 million Joules in its original geotransfer orbit. In a 400 kilometer circular orbit, it has a

24
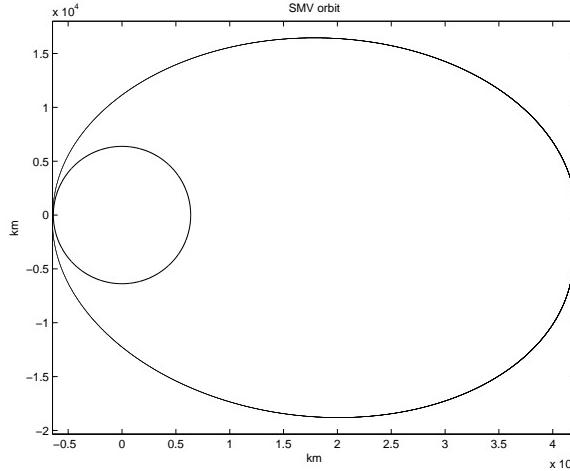
Figure 15:   Lift Perturbed Orbit, Perigee = 45 km

mechanical energy of approximately -29 $(km/s)^2$ and specific kinetic energy of 30 million Joules. This means the SMV must find a means to discard almost 21 $(km/s)^2$ in one orbit. Drag is a nonconservative force that acts in the direction opposite of the SMV's velocity that will bleed away the SMV's energy through heat transfer to the SMV and surrounding air molecules [22, 521]. The acceleration due to planar drag is described by the equation [22, 522]:

$$D = \frac{1}{2} * C_D * \frac{S}{m} * \rho * V_{rel}^2 * \frac{-\vec{V}_{rel}}{\mid V_{rel} \mid} \tag{19}$$

where

C_D = Coefficient of drag

S = Presented area (km^2)

m = SMV mass (kg)

The amount of area that the SMV presents to the oncoming air molecules was determined using a flat plate model for each of the lifting surfaces and main body. At a 21° angle of attack the SMV presents an area of 5.933 m^2. At 50° angle of attack the SMV presents an area of 12.682 m^2, and during a ballistic trajectory, the SMV presents 16.555 m^2.

25

Drag affects the SMV by shortening its semimajor axis and reducing its eccentricity [23, 85]. The simulation was run considering only drag to verify the correct construction of the drag model. Figure 16 displays the SMV's orbit around the earth and verifies the drag model.
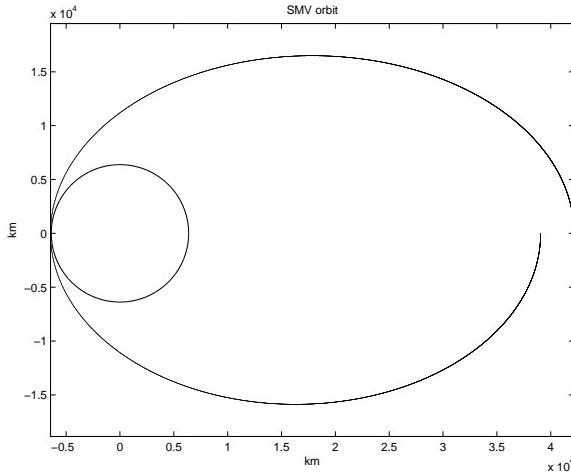
Figure 16:   Drag Perturbed Orbit

Reentry Schemes

This section will describe the two reentry techniques used in this study.

Ballistic Reentry.   When the SMV flies at a 90° angle of attack it has effectively zero lift and plows straight through the atmosphere. The simulation simply integrates the SMV's orbit forward from the target satellite and determines whether or not successful final conditions are met.

"Double-Dip Reentry".   The use of a "Double-Dip" reentry dates back to the American Apollo missions and Soviet Zond capsules. The Apollo and Zond capsules' offset center of mass created a lift vector they could roll to maneuver the capsules in the atmosphere. The capsules plowed into the earth's atmosphere with their lift oriented away from the earth. As their lift began to raise them out of the atmosphere, the capsules rolled their lift vectors towards the earth. Figure 17 displays this ma-

26

neuver [23, 243]. In Figure 17, the horizontal axis represents downrange distance, and the vertical axis represents altitude. X_r and H_r denote the downrange distance and altitude of the spacecraft at rollover.
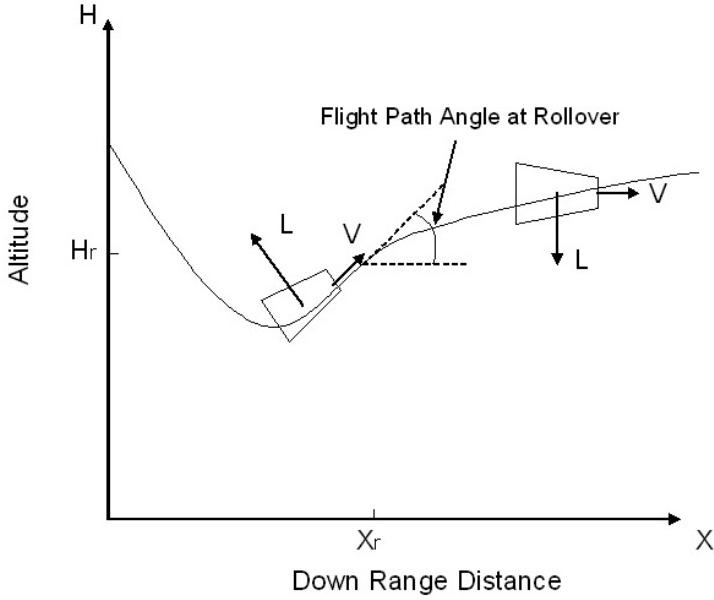
Figure 17:   Potential "Double-Dip" Reentry Flight Profile [23, 243]

Had the capsules not altered their flight profiles after their initial dip into the atmosphere they would have left the atmosphere above escape speed and doomed the astronauts and cosmonauts. As Figure 17 demonstrates, the solution is an easy one. It was necessary to roll the spacecrafts to point their lift vectors towards earth "to help hold the vehicle in the atmosphere while it completes its deceleration" [23, 243]. The capsules performed this maneuver during the upswing portion of their trajectory to avoid rocketing the spacecraft into the ground and killing any of their highly trained space travellers. The roll maneuver is an easy one to perform and has been thoroughly studied.

Now that the logic behind selecting the "Double-Dip" reentry scheme has been explained, the question, "How does one determine the flight path angle at which to roll the SMV?" must be answered. Wiesel's explanation of how to choose that flight path angle will be reviewed. Before beginning, it is important to define the flight path

angle. The flight path angle is the angle between the SMV's velocity vector and the local horizon. Velocity vectors residing below the local horizon result in a negative flight path angle. It is necessary to switch to a flat earth coordinate system at this point in order to determine the flight path angle at which to roll the SMV.

The equations of motion for the SMV must be reconstructed with the flat earth coordinate system. The reconstruction will begin by finding the force of gravity on the SMV. "The apparent gravitational force on the vehicle is given approximately by:" [23, 239]

$$F_g = \frac{\mu \, m}{r^2} - \frac{m \, v^2 \, \cos^2 \gamma}{r} \tag{20}$$

As one can see, "the apparent force of gravity would be negligible compared to the aerodynamic forces on the vehicle during reentry" [23, 239]. For that reason, gravity will be ignored for this formulation. Now, the SMV's equations of motion are: [23, 239]

$$\frac{d\,X}{d\,t} = v \cos \gamma \tag{21}$$

$$\frac{d\,H}{d\,t} = v \sin \gamma \tag{22}$$

$$m \frac{d\,v}{d\,t} = -A_D \tag{23}$$

$$m\,v \frac{d\,\gamma}{d\,t} = L \tag{24}$$

where

X = Downrange Position, (km)

H = Altitude (km)

γ = Flight path angle (rad)

Multiplying the above equations of motion by [23, 240]

$$\frac{d\,t}{d\gamma} + \frac{2m}{C_L A \rho v} \tag{25}$$

28

will allow them to be integrated over the new independent variable, γ. As long as the SMV's flight path angle is a "monotonically increasing function of time" [23, 240], and it is assumed to be, γ is an acceptable independent variable and the SMV's equations of motion while flying right side up are [23, 239]:

$$\frac{dX}{d\gamma} = \frac{1}{K_L} cos\,\gamma\, e^{H/H_0} \tag{26}$$

$$\frac{dH}{d\gamma} = \frac{1}{K_L} sin\,\gamma\, e^{H/H_0} \tag{27}$$

$$\frac{dV}{d\gamma} = -\frac{C_D}{C_L} V \tag{28}$$

where

$$K_L = \frac{C_L\,A\,\rho_0}{2m}$$

Equation 28 can be rearranged, using separation of variables, into the form [23, 240]

$$\frac{dV}{V} = -\frac{C_D}{C_L}\,d\gamma \tag{29}$$

Integrating Equation 29 leads to [23, 240]

$$\int_{V_e}^{V} \frac{dV}{V} = -\frac{C_D}{C_L} \int_{\gamma_e}^{\gamma} d\gamma$$

$$V_{RSU} = V_e\, exp\left(-\frac{C_D}{C_L}(\gamma - \gamma_e)\right) \tag{30}$$

where

V_e = SMV atmospheric entry speed

γ_e = Atmospheric entry flight path angle

V_{RSU} = SMV right side up velocity

Equation 30 holds true until the SMV performs its roll maneuver at γ_r, H_r, and X_r [23, 243]. Realizing that the only change to the equations of motion is the direction

29

of lift allows Equations 26 through 28 to be rewritten as [23, 243]:

$$\frac{dX}{d\gamma} = \frac{1}{K_L} \cos\gamma \, e^{H/H_0} \tag{31}$$

$$\frac{dH}{d\gamma} = \frac{1}{K_L} \sin\gamma \, e^{H/H_0} \tag{32}$$

$$\frac{dV}{d\gamma} = +\frac{C_D}{C_L} V \tag{33}$$

Substituting a velocity at rollover, V_r, as the initial velocity for this portion of the reentry allows Equation 33 to be integrated like Equation 28. The SMV's velocity while upside down can be expressed with the resulting equation [23, 98]:

$$V_{USD} = V_r \, exp\left(\frac{C_D}{C_L}(\gamma - \gamma_r)\right) \tag{34}$$

where

$V_{USD} = $ SMV upside down velocity

Solving for the SMV's right side up rollover velocity

$$V_r = V_e \, exp\left(-\frac{C_D}{C_L}(\gamma_r - \gamma_e)\right) \tag{35}$$

presents a convenient substitution

$$V_{USD} = V_e \, exp\left(-\frac{C_D}{C_L}(\gamma_r - \gamma_e)\right) \times exp\left(\frac{C_D}{C_L}(\gamma - \gamma_r)\right) \tag{36}$$

Solving Equation 36 for the SMV's maximum upside down altitude results in

$$V_{USD}(\gamma = 0) = V_e \, exp\left(-\frac{C_D}{C_L}(2\gamma_r + \gamma_e)\right) \tag{37}$$

A targeted, low earth orbit with an altitude of 300 km would provide a final velocity of about 7.7 km/s per second. This would cause Equation 37 to resemble

$$7.7 = V_e \, exp \left(-\frac{C_D}{C_L}(2\gamma_r + \gamma_e) \right) \tag{38}$$

Immediate inspection of this result would suggest the possibility of picking a final velocity or flight path angle and solving for the remaining variable exists because γ_r is a function of γ_e. Once that was accomplished, integrating backwards in time would provide the mandatory initial conditions; however, choosing physically feasible final conditions is extremely difficult, and for that reason, this method was not tried.

Taking a step back to Equation 27 provides a simpler approach. Separating Equation 27 yields [23, 241]

$$K_L \int_{H_e}^{H} e^{-H/H_0} d\,H = \int_{\gamma_e}^{\gamma} sin\,\gamma\,d\gamma \tag{39}$$

Integrating Equation 39 gives [23, 241]

$$H_{RSU} = H_0 \ln \frac{K_L H_0}{cos\gamma + B} \tag{40}$$

where

$$B = K_L H_0 e^{-H_e/H_0} - cos\gamma_e$$

The variable B is introduced at this point to simplify the notation. As Wiesel points out, "To keep the argument of the logarithm greater than 1 when $\cos \gamma = 1$, we must require that $1 + B < K_L H_0$" [23, 241]. Solving for the upside down altitude by performing a similar integration

$$H_{USD} = H_0 \ln \frac{-K_L H_0}{cos\gamma + B_{USD}} \tag{41}$$

To ensure that H_{USD} is greater than H_0 the natural log in Equation 41 must be positive. This means [23, 244]:

$$B_{USD} \leq -1 \tag{42}$$

Equation 40 and Equation 41 are equal at the rollover point. Setting them equal yields [23, 244]

$$\frac{K_L H_0}{cos\gamma_r + B_{RSU}} = \frac{-K_L H_0}{cos\gamma_r + B_{USD}} \tag{43}$$

Performing some simple algebra produces an equation for B_{USD} [23, 244]:

$$
\begin{aligned}
B_{USD} &= -2\,cos\gamma_r - B_{RSU} \\
B_{USD} &= cos\gamma_e - 2cos\gamma_r - K_L H_0 e^{-H_e/H_0}
\end{aligned}
\tag{44}
$$

substituting Equation 44 into Equation 41 and solving for the flight path angle at rollover in terms of the desired final altitude, H^+ yields [23, 244]:

$$cos\gamma_r = \frac{1}{2}\left[1 + cos\gamma_e + K_L H_0(e^{-H^+/H_0} - e^{-H_e/H_0})\right] \tag{45}$$

Equation 45 can be simplified to

$$cos\gamma_r = \frac{1}{2}\left(1 + cos\gamma_e\right) \tag{46}$$

because H^+ will be well above the atmosphere and H_i can be defined above the atmosphere.

The flight path angle at atmospheric entry is below five degrees for every case. The small flight path angle at entry allows the two cosine terms to be replaced with the first two terms of their Taylor's series [23, 252]. Equation 46 becomes

$$1 - \frac{\gamma_r^2}{2} = \frac{1}{2}\left(1 + 1 - \frac{\gamma_e^2}{2}\right) \tag{47}$$

Simplifying Equation 47 yields

$$\gamma_r^2 = \frac{\gamma_e^2}{2} \tag{48}$$

and because γ_e must be negative for reentry to occur, and γ_r is positive [23, 252]:

$$\gamma_r = \frac{1}{\sqrt{2}} \mid \gamma_e \mid \tag{49}$$

Equation 49 provides a convenient way to find the approximate flight path angle at which to roll the SMV. It will be used in the simulation to do exactly that. Now that an expression for γ_r is available, it can be substituted back into the expression for upside down velocity to solve for the flight path angle at atmospheric entry. For the simulation to work, the final upside down velocity, V_{USD} must be equal to the target circular velocity, V_C. Performing the substitution yields [23, 252]:

$$V_C = V_e \, exp \left[-\frac{C_D}{C_L} \left(\sqrt{2} \mid \gamma_e \mid -\gamma_e \right) \right] \tag{50}$$

rearranging Equation 50 gives [23, 252]:

$$\gamma_e = -\frac{C_L}{C_D} \frac{1}{1 + \sqrt{2}} \ln \left(\frac{V_C}{V_e} \right) \tag{51}$$

Equation 51 can justify this study if it proves that the necessary initial conditions are physically obtainable. The SMV's velocity at atmospheric entry is roughly 10-11.5 kilometers per second while the target final velocity is below 7.75 kilometers per second. Inserting those values into Equation 51 gives a relatively small range of negative flight path angles from -13 to -8.5. This answer is perfect; the flight path angle at atmospheric entry must be negative and small, and it is both. Only numerically integrating the SMV's orbit stands in the way of finding a perigee dip altitude that traps the SMV in a circular, low earth orbit.

Simulation Parameters

After the SMV is built, it will have parameters that cannot be violated or it will be destroyed. This study will propagate each orbit without regard for any physical constraints in order to identify areas of technology that need improvement; however, the option to terminate the current orbit simulation due to violations of the theoretical SMV's constraints exists throughout the entire simulation and can easily be activated. The simulation tracks the SMV's acceleration, heating rate, and altitude along the entire flight.

Accelerations. As it enters the atmosphere, the SMV will experience an increased acceleration due to lift and drag, but it does little good to know just the magnitudes of those accelerations. Most aerodynamic vehicles express their maximum allowable accelerations in terms of a body normal acceleration and a longitudinal acceleration. The Space Shuttle has a maximum normal load of 2.5g [13, 34]. This limit will not be imposed upon the SMV but will be used to judge the SMV's body normal acceleration relative to the Space Shuttle.

The simulation's constant angle of attack assumption allows the accelerations due to lift and drag to be expressed as accelerations in the body normal and longi-tudinal directions by performing some simple trigonometry. As described before, lift acts perpendicular to the vehicle's relative velocity, and drag acts in the direction opposite of the SMV's relative velocity. Figure 18 visually displays this relationship.
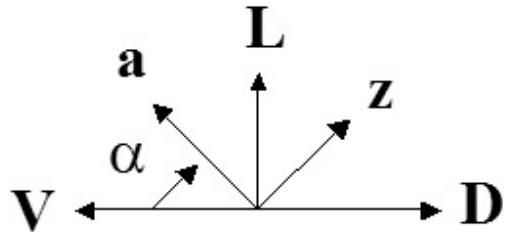
Figure 18:   Aerodynamic Forces on Reentry Vehicle [13, 33]

In Figure 18, $\mathbf{z}$ represents the body normal axis, and $\mathbf{a}$ represents the longitudinal axis of the vehicle. The longitudinal acceleration becomes

$$Longitudinal\ Acceleration = A_{Lift}\sin(\alpha) - A_{Drag}\cos(\alpha) \tag{52}$$

and the body normal acceleration becomes

$$Body\ Normal\ Acceleration = A_{Lift}\cos(\alpha) + A_{Drag}\sin(\alpha) \tag{53}$$

where

α = SMV angle of attack

The body normal and longitudinal accelerations felt by the SMV during successful orbits will be displayed in Chapter IV.

Heating Rate.   Heating rates during atmospheric reentry are one of the largest design constraints for any reentry vehicle. The SMV's heating rate could be quite large because it enters the atmosphere at approximately 11 km/s. Lu provides the heating rate constraint equation [12, 145]

$$\sqrt{\frac{\rho}{\rho_{ref}}}\left(\frac{\sqrt{R_0 g_0}}{v_{ref}}\right)^3 V^3 \leq \frac{\dot{q}_{max}}{C_q} = 3.305 \times 10^9 \tag{54}$$

where

$\rho_{ref} = 1\ kg/m^3$

$v_{ref} = 1$ m/s

$V = v/\sqrt{R_0 g_0}$

$\dot{q}_{max}$ = Maximum stagnation point heating rate (W/m^2)

C_q = Heat flux transmission coefficient (W/m^2)

To maintain continuity with Captain McNabb's previous research, the parameters for maximum stagnation point heating rate and heat flux transmission coefficient are

taken from Lu for a reusable launch vehicle with a stagnation point heating rate based on a reference sphere with a radius of 1 m [12, 145].

$$\dot{q}_{max} = 544{,}300 \; W/m^2$$

$$C_q = 1.65 \times 10^{-4} \, W/m2$$

The SMV's heating rate on successful orbits will be discussed in Chapter IV.

Altitude. Theoretically there is no limit on how deep into the atmosphere the SMV can dip. Once it is built, the SMV could survive any number of reentry profiles, but, because its future parameters are unknown, two altitude floors were considered: 45 km and 70 km. In each case, the simulation was ended if the SMV dipped below the altitude floor. Successful dip altitudes will be discussed in Chapter IV.

III. Model Construction

Chapter Overview

The purpose of this chapter is to explain the methodology behind the simulation's construction. It will detail the simulation's initial and final conditions and discuss the simulation's algorithm.

Initial and Final Conditions

The simulation uses apogee of the SMV's geotransfer orbit as its initial position because the SMV will return immediately after completing its task. The SMV's initial velocity is found by targeting a perigee altitude and substituting it into Equations 57-59. The desired final conditions were formulated keeping the goal of returning the SMV to a near circular, low earth orbit in mind. Several criteria were set to determine whether or not the current orbit was successful. To be considered successful, the SMV's altitude had to be between 184 km and 600 km. The lower altitude was determined from investigating the lower nominal space shuttle mission orbit [19]. In addition to residing within an altitude window, the SMV's velocity had to be within 500 m/s of circular velocity at its current position, and in order to ensure the SMV was in a near circular orbit, success was only declared if its flight path angle was less than 10°. Orbits from the ballistic and "Double-Dip" reentries that meet the above criteria will be discussed in Chapter IV. Any target perigee's orbit that did not meet the success criteria after being integrated through two atmosphere passes was considered unsuccessful.

Simulation Algorithm

The work required to build a robust simulation to model the SMV's return to low Earth orbit is not finished, and, in order to facilitate future work, the algorithm used to create the current simulation's code will be discussed in three steps: a very broad overview, a more detailed description, and, finally, a very detailed description of each function's code. Figure 19 shows the simulation's algorithm.

The simulation is comprised of one main function, SMVdip, and four subfunctions: Cowelldip, RK4dip, Derivdip, and PDerivdip. SMVdip sets up the simulation's initial conditions and calls Cowelldip. Cowelldip contains the "Double-Dip" reentry logic, the perigee and apogee check logic, and the altitude floor check. It also calls RK4dip, the numerical integrator. RK4dip calculates a new state vector using the returned state vector time derivatives it receives from Derivdip and PDerivdip. Derivdip calculates the state vector's time derivative without perturbations. PDerivdip calculates the state vector's time derivative with lift and drag perturbations. SMVdip, Cowelldip, Derivdip, PDerivdip, and RK4dip can be found on the compact disc that accompanies this thesis. A more detailed description of the simulation's five functions is now given.

SMVdip performs several important operations before it begins integrating the SMV's orbit. It sets the simulation's start date and time to 00:00:00 UT on 30 December 2004. The time and date were arbitrarily set, but future simulations that use atmosphere models with seasonal variations will have to be careful in setting the simulation's time and date. SMVdip also sets the integration step size to 1 second. Drag and lift perturbations are turned off or on in the simulation depending upon user specified choices in SMVdip. The circular velocity tolerance and starting perigee altitude are also assigned values.

At this point, SMVdip solves for the orbit's initial position, velocity, and energy and sends them to Cowelldip. Cowelldip will integrate the orbits one at a time until it finds one that meets the desired final conditions. Each time that Cowelldip returns an unsuccessful orbit, SMVdip increases the orbit's target perigee altitude by 0.25 kilometers, recalculates the initial position and velocity, and calls on Cowelldip to integrate the new orbit. If Cowelldip returns a successful orbit, SMVdip plots the results and writes the solution to the designated output file.

Cowelldip begins by initializing a number of logic variables. After those variables are set, it enters a loop that calls RK4dip until the desired stop time is reached. Each

time Cowelldip calls RK4, RK4 returns a new state vector one time step after the last one. Cowelldip uses the new state vector to calculate the flight path angle, and if RK4dip returns a variable indicating an initial encounter with the atmosphere, the flight path angle is stored as the SMV's initial flight path angle. The roll flight path angle is calculated using the initial flight path angle. Once the SMV's flight path angle is greater than the roll flight path angle, Cowelldip rolls the SMV 180 degrees. After each time step, Cowelldip checks for perigee and apogee passage, Earth impact, and successful final conditions.

RK4dip needs the derivative of the state vector with respect to time to calculate the new state vector. RK4dip calls PDerivdip and Derivdip to find the derivative of the state vector. If lift and drag are not being considered, the atmosphere is "off", and Derivdip creates the derivative of the state vector using only gravitational acceleration. Derivdip still calculates lift and drag but only uses them to decide whether or not to turn on the atmosphere. PDerivdip finds the derivative of the state vector using gravity, lift, and drag. PDerivdip also turns "off" the atmosphere if the acceleration due to lift or drag drops below the preset value. Figure 19 gives a visual representation of the simulation algorithm.

Detailed Algorithm

This section will detail each step in the five MATLAB functions beginning with SMVdip. SMVdip begins by converting 00:00:00 UT on 30 December 2004 into a Julian date. It uses a function called JulianDay written by Vallado. The JulianDay function can be found on the compact disc that accompanies this thesis. The variables that are assigned values before SMVdip enters its loop do not require extensive calculations. SMVdip begins its loop by setting up the orbit's initial position and velocity. Doing this requires locating its target. The SMV's target is in geosynchronous orbit with a period equal to twenty-three hours, fifty-six minutes, and roughly four

39

seconds. The target's orbital radius is discerned from the following equation [23, 56]:

$$T = 2\pi \sqrt{\frac{a^3}{\mu}} \qquad (55)$$

where

T = Orbit period (s)

μ = 398600.5 (km^3/s^2)

To simplify the simulation, the SMV's initial position vector is assumed to coincide with its target at its apogee. Constraining the SMV to its orbital plane creates the position vector

$$\vec{r} = \begin{bmatrix} 42164.17 \\ 0 \\ 0 \end{bmatrix} km \qquad (56)$$

SMVdip then reads the desired perigee altitude to dip to, and the simulation uses that information to place the SMV in an equatorial orbit with a semimajor axis described by [22, 104]:

$$a = \frac{R_a + R_p}{2} \qquad (57)$$

where

R_a = Radius of apogee $(42164.17\ km)$

R_p = Radius of perigee

The SMV's energy can then be found by substituting the semimajor axis into the equation [23, 56]:

$$\varepsilon = -\frac{\mu}{2a} \qquad (58)$$

The SMV's velocity at the beginning of the simulation is (Wiesel 1997:51)

$$v = \left(2\varepsilon + \frac{2\mu}{r}\right)^{1/2} \qquad (59)$$

and resides only in the $\hat{e}_y$ direction because the simulation starts at apogee. After calculating the SMV's velocity, SMVdip determines the orbit's end time with the following equation:

$$End\,time = Start\,time + number\,of\,orbits * T/86400 \tag{60}$$

T is found by substituting the SMV's semimajor axis into Equation 55, and the number of orbits is a real number entered by the user. The simulation can integrate forward or backward in time. At this point, SMVdip calls Cowelldip.

Cowelldip starts by initializing logic switches and then immediately calls RK4dip. Cowelldip tells RK4dip the current state vector, current time, which perturbations to consider, and the direction of lift. In order to calculate a new state vector, RK4dip calls either Derivdip or PDerivdip four times at three different time steps: once at the current time, twice at the current time plus half the step size, and once at the current time plus the entire step size. Both subfunctions calculate the accelerations due to gravity, lift, and drag at the SMV's current position and velocity to formulate the state vector's time derivative.

PDerivdip begins by calculating the gravitational acceleration with the equation

$$\dot{\vec{X}} = \begin{bmatrix} \dot{x} \\ \dot{y} \\ \dot{z} \\ x * \frac{-\mu}{r^3} \\ y * \frac{-\mu}{r^3} \\ z * \frac{-\mu}{r^3} \end{bmatrix} \tag{61}$$

Once PDerivdip updates the state vector's time derivative, it must find lift and drag in order to add them to the time derivative. The SMV's velocity relative to the atmosphere must be found. It is found by performing a vector cross product with the Earth's rotation vector and the SMV's position vector. Stated in equation form

$$\vec{V}_{atmosphere} = \vec{\omega}_{\oplus} \times \vec{r} \qquad (62)$$

where

$$\vec{\omega}_{\oplus} = \text{Earth's rotation vector} \begin{bmatrix} 0 \\ 0 \\ 0.000072921151467 \end{bmatrix} \text{r/s}$$

The SMV's velocity relative to the atmosphere is computed with the equation:

$$\vec{V}_{rel} = \vec{v} - \vec{V}_{atmosphere} \qquad (63)$$

The next step in computing the lift and drag is to find the density of the atmosphere. PDerivdip and Derivdip send the SMV's altitude to a subroutine called ATMOSPHERE2D that returns the atmospheric density at that altitude. ATMOSPHERE2D can be found on the compact disc that accompanies this thesis. Now that the SMV's velocity relative to the atmosphere and atmospheric density are known, the acceleration due to drag can be computed using Equation 19.

Once drag is computed, PDerivdip adds it to the state vector's time derivative. Now,

$$\dot{\vec{X}} = \begin{bmatrix} \dot{x} \\ \dot{y} \\ \dot{z} \\ x * \frac{-\mu}{r^3} + A_D \\ y * \frac{-\mu}{r^3} + A_D \\ z * \frac{-\mu}{r^3} + A_D \end{bmatrix} \qquad (64)$$

Derivdip also calculates the SMV's drag but does not add it to the state vector's time derivative. It finds drag only to determine whether or not to turn "on" the atmosphere.

PDerivdip and Derivdip construct the lift acceleration vector next. Before the SMV rolls over, the lift vector's direction is determined by performing a vector cross

42

product with the SMV's relative velocity and a unit vector in the $\vec{e}_z$ direction. The direction of the SMV's lift vector is then:

$$\vec{L} = \vec{V}_{rel} \times \vec{k} \tag{65}$$

where

$$\vec{k} = \begin{bmatrix} 0 \\ 0 \\ 1 \end{bmatrix}$$

Multiplying out the cross product reveals that the lift vector points away from the Earth. $\vec{L}$ is turned into a unit vector with the following equation:

$$\hat{L} = \frac{\vec{L}}{\mid L \mid} \tag{66}$$

Once the SMV has rolled over, Equation 65 becomes

$$\vec{L} = \vec{V}_{rel} \times -\vec{k} \tag{67}$$

The lift direction unit vector computation does not change from above. Once the direction of lift is determined, the lift magnitude is multiplied by the lift direction unit vector to find the inertial acceleration experienced by the SMV. The state vector's time derivative becomes

$$\dot{\vec{X}} = \begin{bmatrix} \dot{x} \\ \dot{y} \\ \dot{z} \\ x * \frac{-\mu}{r^3} + A_D + A_L \\ y * \frac{-\mu}{r^3} + A_D + A_L \\ z * \frac{-\mu}{r^3} + A_D + A_L \end{bmatrix} \tag{68}$$

43

Like before, Derivdip also computes the SMV's lift but uses it only to determine whether or not to turn "on" the atmosphere. If the SMV's constraints are being considered, PDerivdip compares the magnitude of the lift and drag accelerations to the parameters previously discussed. If those accelerations surpass the limits, flags in PDerivdip note that failure and force the simulation to start over with the next perigee altitude. Because Derivdip is only used when the SMV is above any noticeable atmosphere, it does not contain the logic flags that signal constraint violation.

Derivdip's and PDerivdip's final task is to calculate the heating rate. Equation 54 is simplified to

$$Heating\ Rate = \sqrt{\rho}\ |\ V_{rel}\ |^3 \tag{69}$$

If SMV constraints are being considered and the heating rate exceeds the maximum discussed in Chapter II, the simulation is ended, and the next perigee altitude is attempted.

PDerivdip and Derivdip return the state vector's time derivative at three different times to RK4dip; RK4dip then calculates the new state vector using the equation:

$$\vec{X2} = \vec{X} + (\vec{K1} + 2.0 * (\vec{K2} + \vec{K3}) + Dt * \vec{K4})/6.0 \tag{70}$$

where

Dt = Integration step size

K1 = $Dt * \dot{\vec{X}}(t_0, X_0)$

K2 = $Dt * \dot{\vec{X}}(t_0 + dt/2, X_0 + Dt/2 * K1/Dt)$

K3 = $Dt * \dot{\vec{X}}(t_0 + Dt/2, X_0 + Dt/2 * K2/Dt)$

K4 = $Dt * \dot{\vec{X}}(t_0 + Dt, X_0 + Dt * K3)$

After RK4dip returns the new state vector, Cowelldip updates the time and finds the SMV's flight path angle by calling a function called vecangle. Vecangle uses the

equation [11, 409]:

$$\cos^{-1}\gamma = \frac{\vec{b} \cdot \vec{v}}{\mid \vec{b} \mid \mid \vec{v} \mid} \tag{71}$$

where

$\vec{b} =$ Vector in orbit plane perpendicular to SMV radius vector

Cowelldip corrects the sign of vecangle's returned flight path angle by multiplying it with a logic variable that equals negative one while the SMV travels from apogee to perigee and positive one while it travels from perigee to apogee. The first time Derivdip detects noticeable accelerations from the atmosphere, Cowelldip assigns the current flight path angle value as the atmospheric entry flight path angle. The roll over flight path angle is determined using the equation [23, 252]:

$$\gamma_r = \frac{1}{\sqrt{2}} * abs(\gamma_e) \tag{72}$$

When the SMV's flight path angle exceeds the roll over flight path angle, Cowelldip rolls the SMV by telling PDerivdip to use Equation 67 in place of Equation 65 when calculating lift. After Cowelldip checks for roll over it determines if the SMV's orbit meets the desired final conditions. If the SMV has an altitude between 184 km and 600 km, a flight path angle below 10 degrees, and a velocity less than 500 m/s smaller or greater than circular speed at its current altitude that orbit was successful. Next Cowelldip performs an apogee and perigee check and an Earth impact check. If the SMV has passed perigee twice or hit the Earth, Cowelldip stops the integration, and SMVdip picks a new perigee altitude target. Cowelldip loops until success is acheived, the SMV hits the Earth, or the SMV passes perigee twice. Cowelldip reports the status of the current orbit to SMVdip once it is finished integrating. If the pergiee guess was successful, SMVdip will plot the SMV's orbit around the Earth and update the output file. If the perigee guess was unsuccessful, SMVdip will increase the perigee altitude by 250 meters and start again.

SMV dip
- Set start date
- Set integration step size
- Turn lift and drag on/off
- Set velocity tolerance
- Set starting perigee altitude
- Loop until Cowelldip returns successful orbit
    - Find semimajor axis
    - Find energy
    - Set initial position and velocity
    - Find orbit period
    - Set integration stop time
    - Call Cowelldip
    - If current guess was unsuccessful add 250 meters to perigee altitude
    - If current guess worked end loop
- Plot results

Cowelldip
- Loop while Julian date < simulation end date
    - Call RK4dip
    - Find flight path angle
    - Set initial atmospheric entry flight path angle when atmosphere turned on the first time
    - Set roll over flight path angle
    - If flight path angle greater than roll over flight path angle roll SMV
    - If perigee/apogee passed since last time step change flight path angle sign
    - If SMV impacts Earth end Cowelldip and return to SMVdip
    - If SMV parameters violated end Cowelldip and return to SMVdip (Can be turned off)
    - If successful final conditions are met end Cowelldip
    - Update time
- Return variable denoting success or failure to SMVdip

RK4dip
- If perturbations are on call PDerivdip
- If perturbations are off call Derivdip
- Calculate new state vector
- Return new state vector to Cowelldip

PDerivdip
- Find gravitational acceleration
- Set SMV's angle of attack and reference areas
- Solve for lift, drag, and heating rate
- Update state vecor's time derivative with gravity, lift, and drag
- Check for constraint violations
- If lift or drag below tolerance turn off atmosphere
- Return time derivative of state vector to RK4dip

Derivdip
- Find gravitational acceleration
- Set SMV's angle of attack and reference areas
- Solve for lift and drag
- Update state vector's time derivative with gravity
- If lift or drag above tolerance turn on atmosphere
- Return time derivative of state vector to RK4dip

Figure 19:   Simulation Algorithm

46

IV. Results

Chapter Overview

This chapter will present the results obtained from numerically integrating the SMV's orbit using both reentry schemes. Successful one and two pass orbits for each reentry scheme will be examined. The effects of increased atmospheric density on the successful perigee windows will also be examined.

Bifurcation

Aerobraking the SMV into a circular, low earth orbit in one or two passes requires dipping deep into earth's atmosphere. As the SMV dips its perigee deeper into earth's atmosphere, it decelerates faster and faster; however, this increased deceleration does not come without risks. If the SMV dips too deeply into the atmosphere, it will not come out. The bifurcation point is the lowest altitude that, when dipped to, allows the SMV to exit the atmosphere. If the SMV were to dip any lower, it would be forced to reenter and land directly from geotransfer orbit. Because this study aims to return the SMV into a low earth, phasing orbit, dipping to altitudes below the bifurcation point were not considered. Identifying the bifurcation point for each angle of attack and altitude floor identifies the beginning of potential solution windows. Table 3 shows the bifurcation altitudes that were found using empirical analysis for each angle of attack and altitude floor. The 21° and 50° angle of attack bifurcation points were found using the "Double-Dip" reentry flight profile. The 90° angle of attack results represent the ballistic reentry flight profile. Two altitude floors, 45 and 70 km, were used in the simulation, but because the 70 km altitude floor did not produce any solutions, those results will not be shown.

Table 3:   Bifurcation Altitudes For 21°, 50°, and 90° Angle of Attack

Altitude Floor	21°	50°	90°
45 km	49.6 km	48.9 km	76 km

Successful Simulations

This section will detail the successful perigee altitude windows for each reentry profile. Because no successful 21° angle of attack perigee altitudes were found, 21° angle of attack orbits will no longer be mentioned in this chapter.

Ballistic Reentry. Table 4 displays the successful perigee altitude windows for one and two pass ballistic reentry. In Table 4, the target altitudes refer to the perigee altitudes used to formulate the SMV's unperturbed velocity. Once the SMV's orbit was integrated with perturbations, a true perigee altitude was produced for each target pergiee.

Table 4: Successful Ballistic Reentry Altitude Windows

Number of Passes	Target Altitudes (km)	Actual Altitudes (km)
1	67.75 - 69.15	66.801 - 68.449
2	72.55 73.75	72.226 - 73.445

The lowest and highest one pass solutions, along with the lowest and highest two pass solutions, will be presented because they most likely contain the lower and upper limits for the SMV's heating rate and accelerations. Table 5 gives the SMV's altitude, instantaneous velocity, and heating rate at its first perigee passage for each altitude. Table 6 lists the SMV's experienced accelerations at its first perigee.

Table 5: Instantaneous Characteristics at Perigee for Ballistic Reentry

Altitude (km)	Passes	Velocity (km/s)	Heating Rate (W/m^2)
66.801	1	9.240	1005072.61
68.449	1	9.506	974556.91
72.226	2	9.889	832638.55
73.445	2	9.969	779789.93

Table 6 gives the maximum body normal acceleration but does not give an accurate representation of the longitudinal acceleration experienced by the SMV. This occurs because the acceleration due to drag acts only in the body normal direction at perigee.

Table 6:   Instantaneous Accelerations at Perigee for Ballistic Reentry

Altitude (km)	Body Normal (g's)	Longitudinal (g's)
66.801	4.388	0
68.449	3.651	0
72.226	2.221	0
73.445	1.863	0

Table 7 shows the approximate maximum value for longitudinal acceleration during the maneuver in g's.

Table 7:   Approximate Maximum Longitudinal Acceleration for Ballistic Reentry

Perigee Altitude (km)	Passes	Longitudinal Acceleration (g's)
66.801	1	2.75
68.449	1	0.8
72.226	2	1.4
73.445	2	1.1

It is also important to analyze the successful final conditions of each perigee's orbit. Table 8 details the SMV's final altitude, the difference between its velocity and circular velocity at its current altitude, and eccentricity.

Table 8:   Final Conditions for Ballistic Reentry

	Altitude (km)	$\mid V_{circ} - V_{actual} \mid$ (km/s)	Eccentricity
One pass bottom	184.11	.0266	.0342
One pass top	598.22	.1971	.2021
Two pass bottom	184.11	.0328	.0179
Two pass top	545.78	.4999	.1954

These results show that as the SMV dips lower into the atmosphere, it gets closer to leaving the atmosphere in a circular orbit but suffers larger accelerations and heating rates. This condition causes choosing a perigee altitude to become a trade off between constructing an incredibly strong reentry vehicle that needs less fuel to complete its reentry after aerobraking and constructing a less sturdy vehicle that must retain more fuel to correct its reentry velocity.

49

Figures 20-26 show the 66.801 km perigee ballistic reentry orbit, heating rate, velocity, altitude, acceleration in the body normal direction, and the magnitude of drag through the entire flight. Figures 28-34 show the same graphs for the 68.449 km perigee ballistic reentry. Acceleration due to lift in the ballistic reentry is ignored because it equals zero for the entire maneuver. Figures 36 -43 show the same graphs for the 72.226 km perigee, two pass ballistic reentry, and Figures 44-51 show the same graphs for the 73.445 km perigee, two pass ballistic reentry. All of the following figures can be found in Appendix A.

Investigation of Figures 20-26 show that the entire maneuver is accomplished in less than six hours. Unfortunately, Figure 24 reveals that the SMV's heating rate during its 66.801 km ballistic pass exceeds the $\dot{q}_{max}$ established in Chapter II by a factor of 2. Figure 32 shows that the 68.449 km ballistic pass exceeds the heating rate constraint by a factor of roughly 1.8. The two pass solutions fare slightly better by only violating the heating constraint by a factor of approximately 1.5. If the SMV's heating rate limit resembles Lu's constraint, current thermal protection system technology will not suffice in returning the SMV to low earth orbit in one or two passes.

"Double-Dip" success. The "Double-Dip" reentry produced successful one and two pass reentries. Table 9 displays the successful perigee altitude windows for one and two pass "Double-Dip" reentries. In Table 9, the target altitudes refer to the perigee altitudes used to formulate the SMV's unperturbed velocity. Once the SMV's orbit was integrated with perturbations, a true perigee altitude was produced for each target pergiee.

Table 9:   Successful "Double-Dip" Reentry Altitude Windows

Number of Passes	Target Altitudes (km)	Actual Altitudes (km)
1	73 - 77.85	62.416 - 64.823
2	77.85 - 78.1	64.823 - 64.962

The lowest one pass solution and the highest two pass solution, along with the highest one pass solution, will be investigated in detail. Table 10 gives the SMV's altitude, velocity, and heating rate at its first perigee passage for each altitude.

Table 10:   Perigee Characteristics for "Double-Dip" Reentry

Altitude (km)	Passes	Velocity (km/s)	Heating Rate (W/m^2)
62.416	1	9.240	1413122.75
64.8232	1	9.482	1277526.36
64.962	2	9.494	1269114.22

Table 11 lists the SMV's experienced accelerations at its first perigee. Displaying the accelerations due to lift and drag will help determine which force contributes the greatest to the SMV's acceleration.

Table 11:   Perigee Accelerations for "Double-Dip" Reentry

Altitude (km)	Body Normal (g's)	Longitudinal (g's)	Lift (g's)	Drag (g's)
62.416	3.028	-1.549	.764	3.313
64.823	2.23	1.142	.5606	2.446
64.961	2.19	-1.120	.550	2.398

Table 12 details the final conditions of each "Double-Dip" orbit. Figures 52-78 give the SMV's orbit, heating rate, velocity, altitude, acceleration in the body normal direction, acceleration in the longitudinal body direction, the magnitude of lift acceleration, and the magnitude of drag acceleration through the entire flight for the 62.416, 64.823, and 64.962 km perigee "Double-Dip" reentries. Examination of those graphs shows that for the lowest possible "Double-Dip" reentry, the SMV violates the maximum heating rate constraint by a factor of roughly 2.75. The increased heating rate during the "Double-Dip" reentry is caused by its lower dip into the atmosphere. Stagnation point heating analysis would reveal an even greater jump in the heating rate of the "Double-Dip" reentry compared to the ballistic reentry because of its reduced radius of curvature. Figures 59, 68, and 77 show the change in the SMV's body normal acceleration as its perigee is raised to the highest two pass altitude.

Table 12:   Final Conditions for "Double-Dip" Reentry

	Altitude (km)	$\mid V_{circ} - V_{actual} \mid$ (km/s)	Eccentricity
One pass bottom	184.042	.0845	.0520
One pass top	598.218	.1930	.1993
Two pass top	597.942	.1934	.1995

The results from this study can be compared to the Powell study to establish a comparison between the two conceptual reentry vehicles. Figure 79 reveals that the high lift-to-drag AOTV must dip to roughly 54 km, 8.4 km deeper into the atmosphere than the lowest "Double-Dip" reentry. This mission requirement most likely stems from the fact that the AOTV was to be a much heavier vehicle than the SMV. It had to dip deeper into the atmosphere in order to be captured in a low earth orbit. Dipping deeper into the atmosphere should cause the AOTV's heating rate to exceed the SMV's heating rate. Figure 81 shows, once the units are converted, that the AOTV's heating rate does indeed surpass the SMV's envisioned heating rate and exceeds Lu's constraint by a factor of 11. Figure 80 shows that two vehicles experience approximately the same magnitude of accelerations.

Atmospheric Sensitivity

The ballistic and "Double-Dip" simulations were run a second time with a five percent increase in their atmospheric densities to demonstrate the perigee windows' susceptibility to atmospheric fluctuations. Table 13 shows the new successful perigee windows. Increasing the atmospheric density by five percent had negative effects on

Table 13:   Perigee Windows for Increased Atmospheric Density

Type of Reentry	Number of Passes	Altitudes (km)
Ballistic	1	67.046 - 68.513
Ballistic	2	72.631 - 73.691
"Double-Dip"	1	63.202 - 65.228
"Double-Dip"	2	65.228 - 65.362

every perigee window because everyone of them got smaller. Table 14 shows these effects.

Table 14:   Effects of Increased Atmosphere on Perigee Windows

Type of Orbit	Vertical Change (km)	Width Change (km)
1 Pass Ballistic	.245 Up	Shrunk by .181
2 Pass Ballistic	.405 Up	Shrunk by .159
1 Pass "Double-Dip"	.786 Up	Shrunk by .381
2 Pass "Double-Dip"	.405 Up	Shrunk by .005

The crux of the aerobraking maneuver is the SMV's burn at apogee to lower its perigee to the right altitude. As the perigee windows get smaller, performing a burn at apogee that leads to a successful orbit becomes increasingly difficult. Table 15 displays the differences between the ΔV's required to dip to the bottom of the perigee window and the ΔV's required to dip to the top of the perigee window.

Table 15: ΔV Requirements with Original Atmospheric Density

Reentry Type	Perigee Window (km)	$\Delta V_{bottom} - \Delta V_{top}$ (km/s)
Ballistic	66.801-68.449	.000149
Ballistic	72.226-73.445	.000122
"Double-Dip"	62.416-64.823	.000516
"Double-Dip"	64.823-64.962	.000027

The increased atmosphere shrinks the successful perigee window, and, as a result, increases the required accuracy of the burn at apogee. Table 16 shows the differences between the ΔV's required to dip to the bottom of the perigee window and the ΔV's required to dip to the top of the perigee window with an increased atmospheric density.

The burn at apogee to enter a successful orbit with a known atmospheric density requires a great deal of precision. The largest ΔV window spans only .5 m/s, and the smallest ΔV window ranges only .027 m/s. Any error in the apogee burn greater than the ΔV window will send the SMV into an unsuccessful orbit. The required ΔV accuracy for a burn with uncertain atmospheric density becomes even greater.

Table 16: ΔV Requirements with Increased Atmospheric Density

Reentry Type	Perigee Window (km)	$\Delta V_{bottom} - \Delta V_{top}$ (km/s)
Ballistic	67.046-68.513	.000133
Ballistic	72.631-73.691	.000106
"Double-Dip"	63.202-65.228	.000425
"Double-Dip"	65.228-65.362	.000026

The change in both perigee windows and the required burn accuracy implies that a small error or drastic change in atmospheric density during aerobraking would lead to mission failure. At this point, the need for an active control system aboard the SMV becomes glaringly obvious.

54

V. Conclusions and Recommendations

The purpose of this study was to prove that a theoretical SMV could maneuver to geotransfer orbit, perform a task, and quickly return to low earth orbit in no more than two atmosphere passes with its advertised ΔV of 3.2 km/s by aerobraking. This was done by numerically integrating the SMV's orbit considering the effects of lift and drag around a planar earth model. Now that this task has been completed, the following conclusions can be drawn from the results provided in Chapter IV. This chapter will end with recommendations for future study.

Conclusions

As proven in Chapter IV, the SMV can maneuver to geotransfer orbit, perform a task, and swiftly return to a near circular, low earth orbit using aerobraking. This ability justifies the required research and development costs because it will greatly increase the SMV's mission capabilities. However, the SMV's ability to swiftly return to earth with a minimal amount of ΔV comes at a high price. The SMV experiences extremely large heating rates that will require a thermal protection system that outperforms today's state-of-the-art thermal protection systems, and the rocket burn needed to enter a successful aerobraking orbit requires an accuracy unavailable from today's rocket engines. It is, however, possible to overcome the hurdle posed by the required burn accuracy by incorporating a number of smaller correctional burns as part of an active control system as the SMV approaches perigee.

The ballistic and "Double-Dip" reentries have significantly different characteristics. The "Double-Dip" reentry's perigee window is significantly larger than the ballistic reentry's perigee window, and that allows for greater uncertainty in the rocket burn, but it's greatest heating rate is larger by approximately 400,000 W/m^2. While the "Double-Dip" reentry may have the largest perigee window, the ballistic reentry produces the orbit with the best, near circular, final conditions. The lack of an undisputed champion between the two reentries makes finding a solution that combines the best features of each an interesting and worthwhile problem.

Recommendations

1. This study depended on keeping the SMV's angle of attack constant. Future study of this problem should include varying the angle of attack as a function of velocity or experienced drag.

2. The model can be expanded to handle three dimensional cases. One of the needed improvements include freeing the lift vector from the position-velocity plane. Freeing the lift vector from the position-velocity plane will require developing expressions for the SMV's roll, pitch, and yaw. Changing the SMV's orientation as it travels through the atmosphere will also change its lift and drag reference areas. Expressions for those must also be developed. Once expressions were developed for the SMV's three controllable angles, it would be more advantageous to handle the reentry as a two-point boundary problem. The simulation would then return the ideal flight trajectory with detailed profiles of its roll, pitch, yaw, and angle of attack during the flight.

3. Future users of this simulation might wish to include smaller perturbations to more accurately model the SMV's orbit. The higher order geopotential terms, third-body gravitational effects from the sun and moon, and solar radiation are just a few of the potential perturbations that could be included.

4. Any future research using this simulation should consider working in a different programming language. MATLAB is a user friendly programming language, but any advantages in programming ease are lost because of slow computation speed.

5. The vehicle parameters used in this study are all estimates for the SMV. When a prototype is built, more accurate information will be available to researchers. Improvements in the SMV's aerodynamic properties should be included as they are made available to the research community.
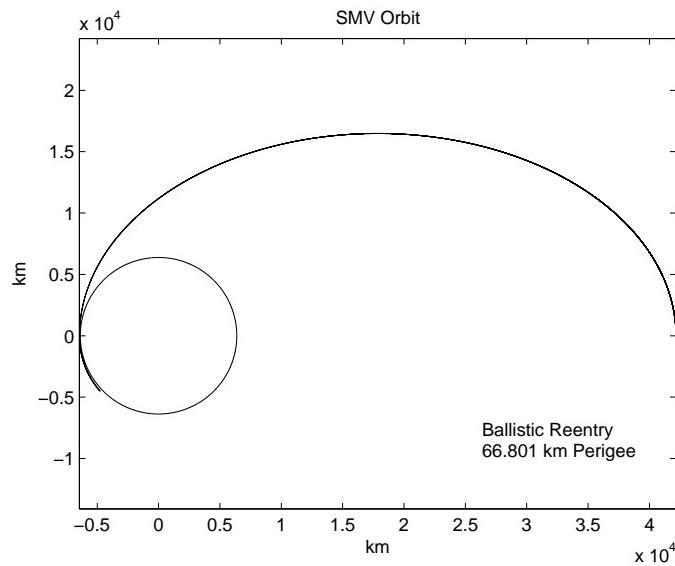
Figure 20:   Orbit for Ballistic Reentry, 66.801 km Perigee
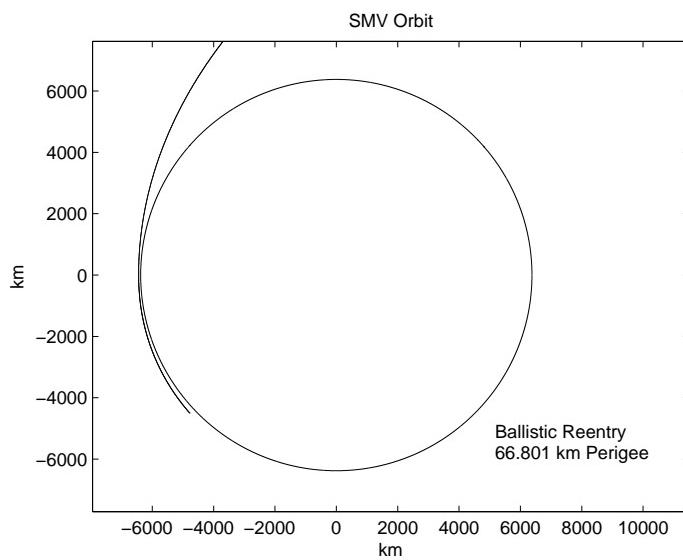
Figure 21:   Near Earth Portion of Orbit for Ballistic Reentry, 66.801 km Perigee
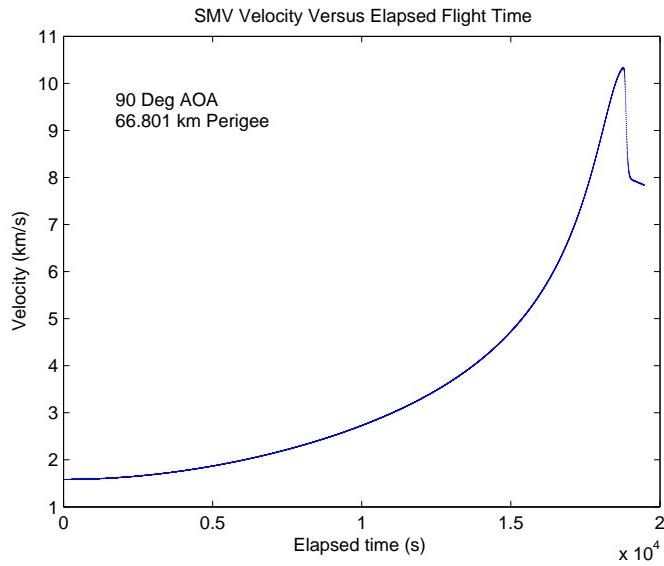
Figure 22:   SMV Velocity Versus Elapsed Time for Ballistic Reentry, 66.801 km Perigee
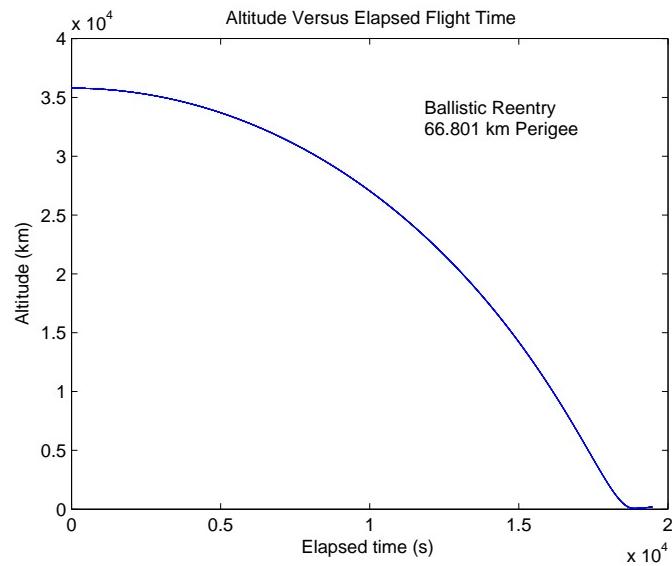

Figure 23:   SMV Altitude Versus Elapsed Time for Ballistic Reentry, 66.801 km Perigee
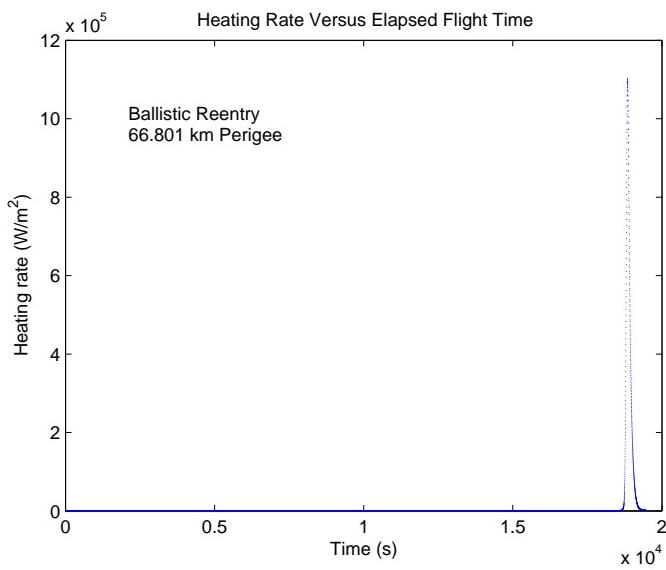
Figure 24:   SMV Heating Rate Versus Elapsed Time for Ballistic Reentry, 66.801 km Perigee
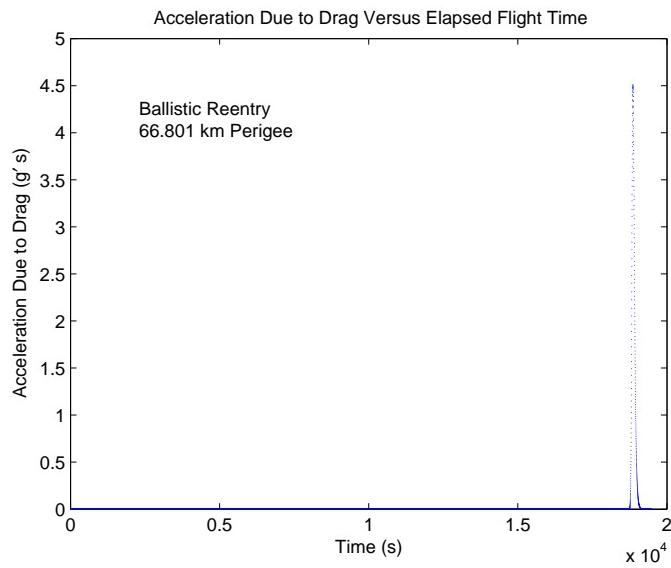

Figure 25:   Acceleration Due to Drag Versus Elapsed Time for Ballistic Reentry, 66.801 km Perigee
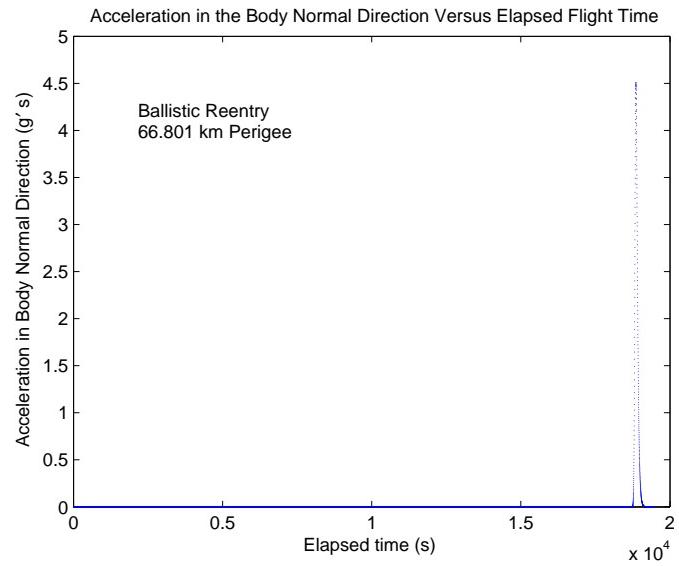
Figure 26:   Acceleration in Body Normal Direction Versus Elapsed Time for Ballistic Reentry, 66.801 km Perigee
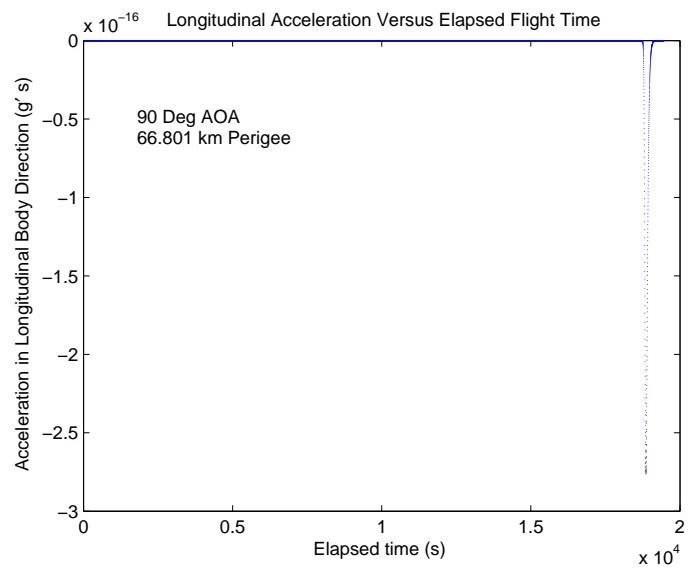
Figure 27:   Acceleration in Longitudinal Direction Versus Elapsed Time for Ballistic Reentry, 66.801 km Perigee
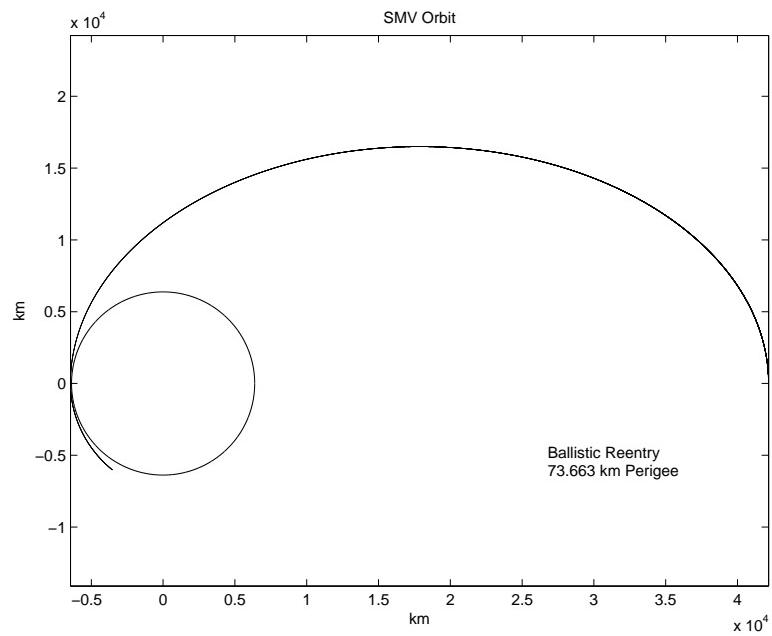
Figure 28:   Orbit for Ballistic Reentry, 68.449 km Perigee
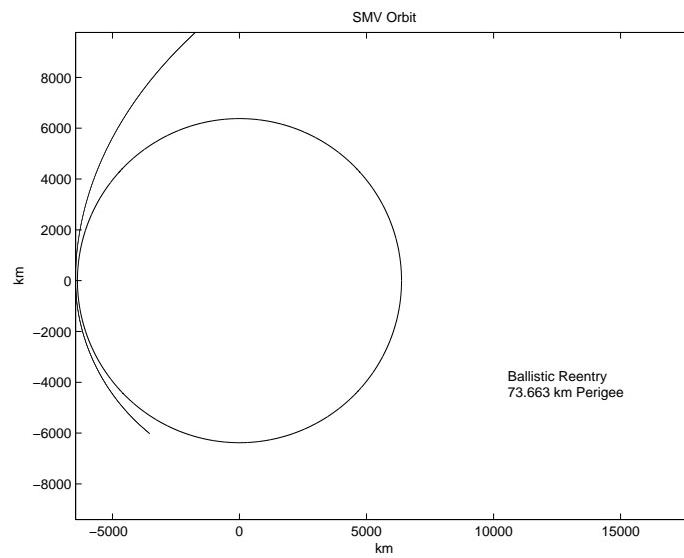
Figure 29:   Near Earth Portion of Orbit for Ballistic Reentry, 68.449 km Perigee
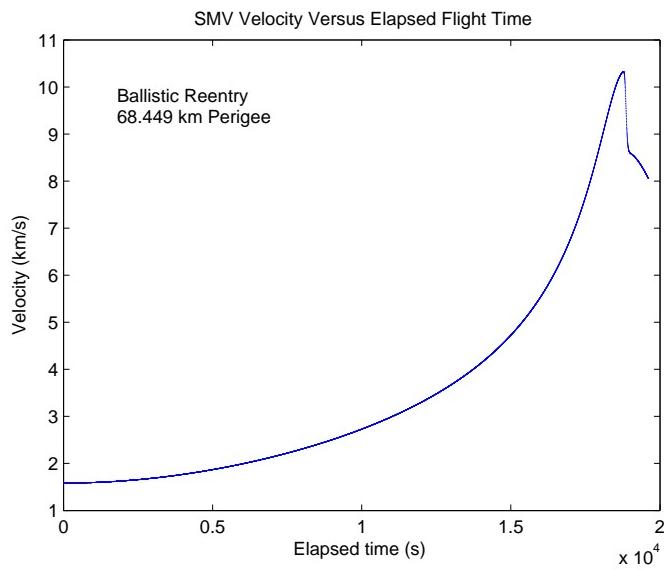
Figure 30:   SMV Velocity Versus Elapsed Time for Ballistic Reentry, 68.449 km
Perigee
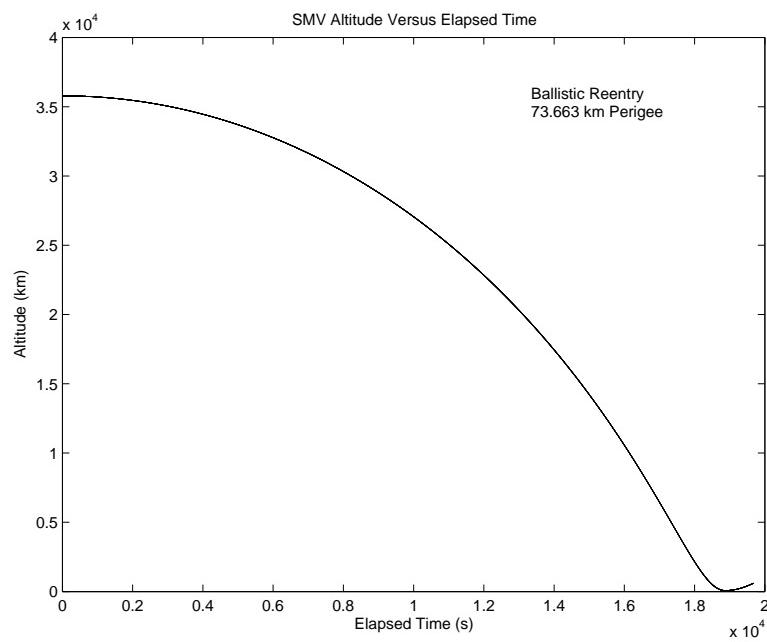
Figure 31:   SMV Altitude Versus Elapsed Time for Ballistic Reentry, 68.449 km
Perigee
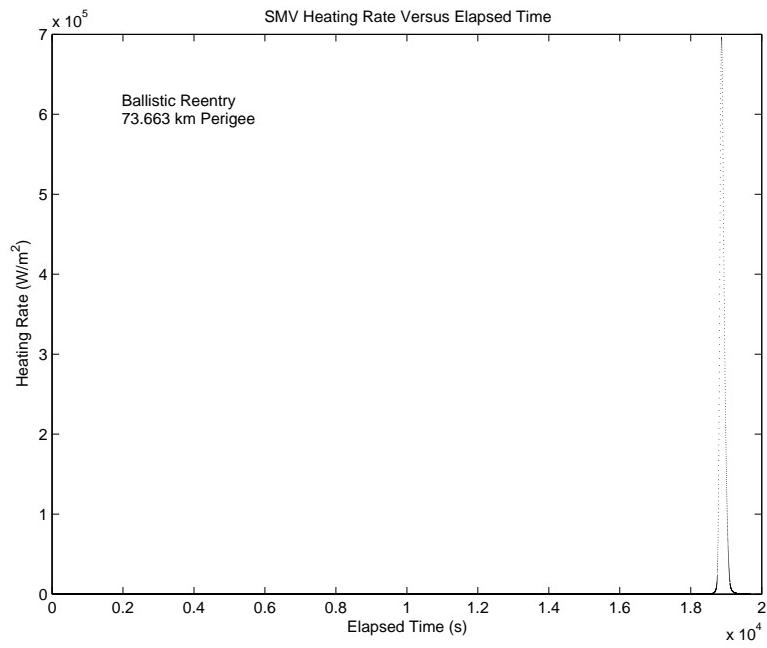
Figure 32:   SMV Heating Rate Versus Elapsed Time for Ballistic Reentry, 68.449
km Perigee
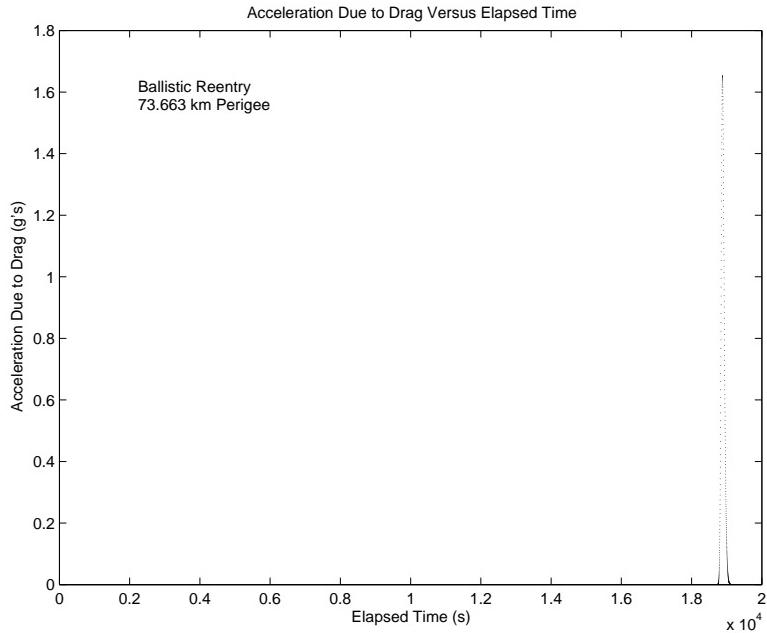
Figure 33:   Acceleration Due to Drag Versus Elapsed Time for Ballistic Reentry,
68.449 km Perigee
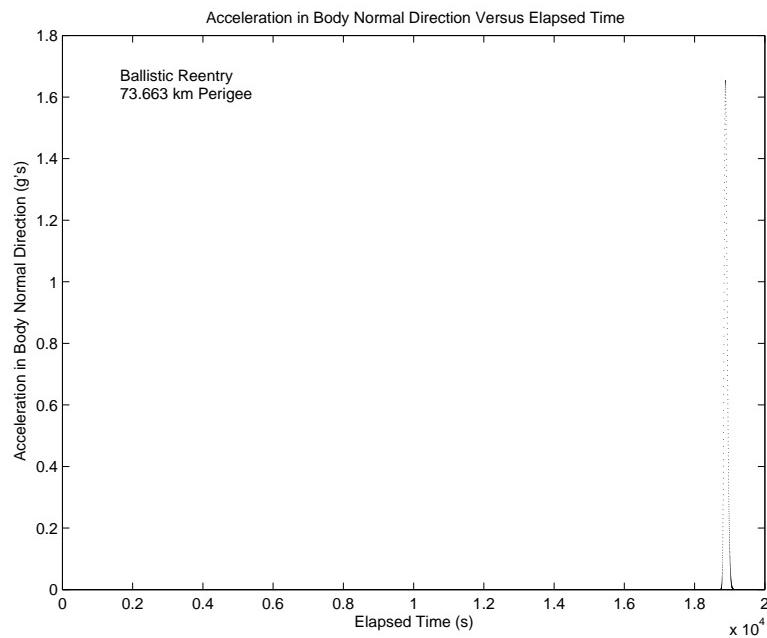
Figure 34: Acceleration in Body Normal Direction Versus Elapsed Time for Ballistic Reentry, 68.449 km Perigee
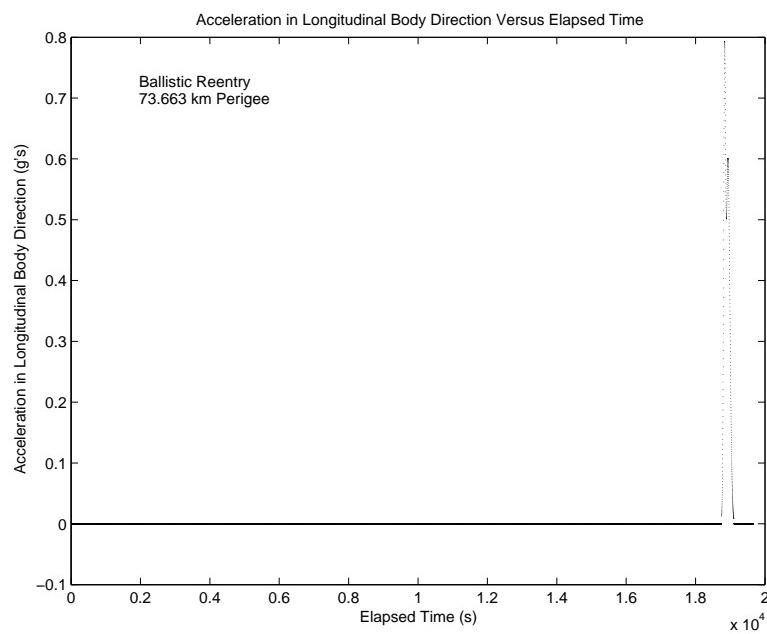

Figure 35: Acceleration in Longitudinal Direction Versus Elapsed Time for Ballistic Reentry, 68.449 km Perigee
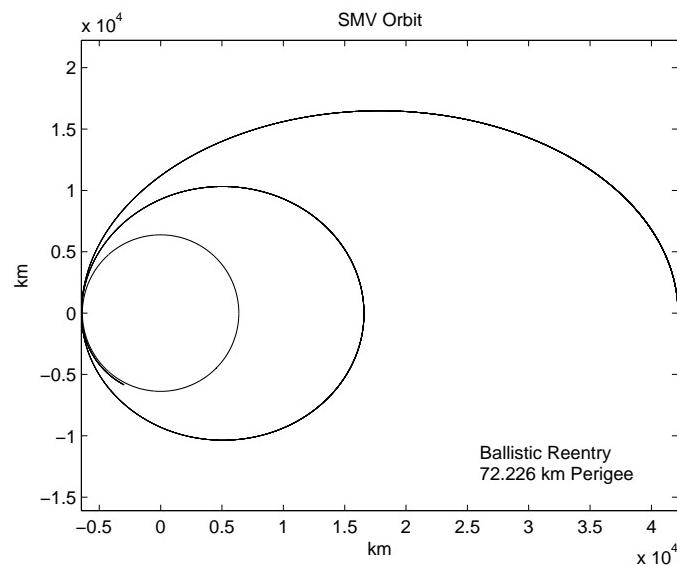
Figure 36:   Orbit for Ballistic Reentry, 72.226 km Perigee
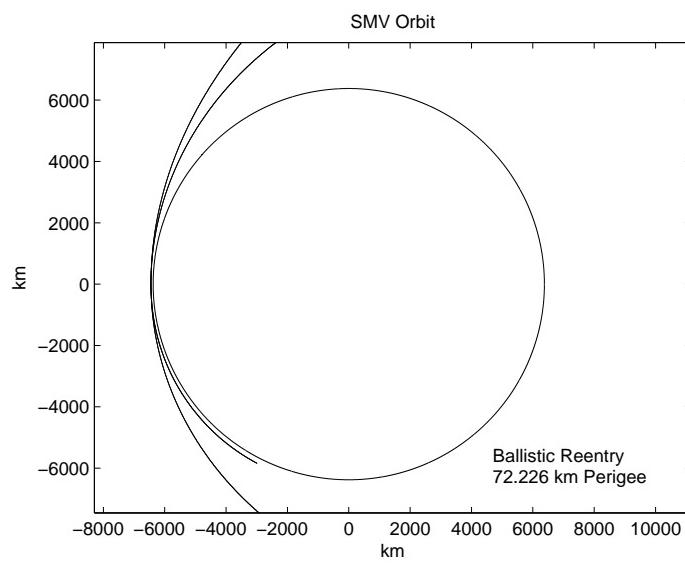
Figure 37:   Near Earth Portion of Orbit for Ballistic Reentry, 72.226 km Perigee

65
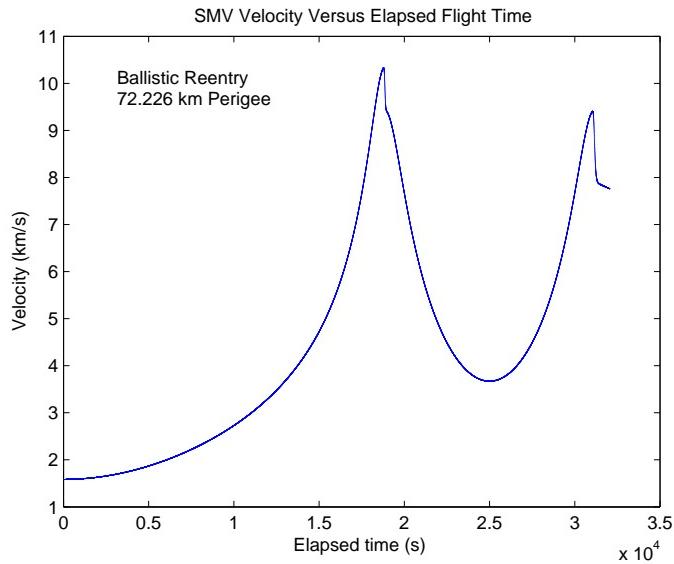
Figure 38:   SMV Velocity Versus Elapsed Time for Ballistic Reentry, 72.226 km Perigee
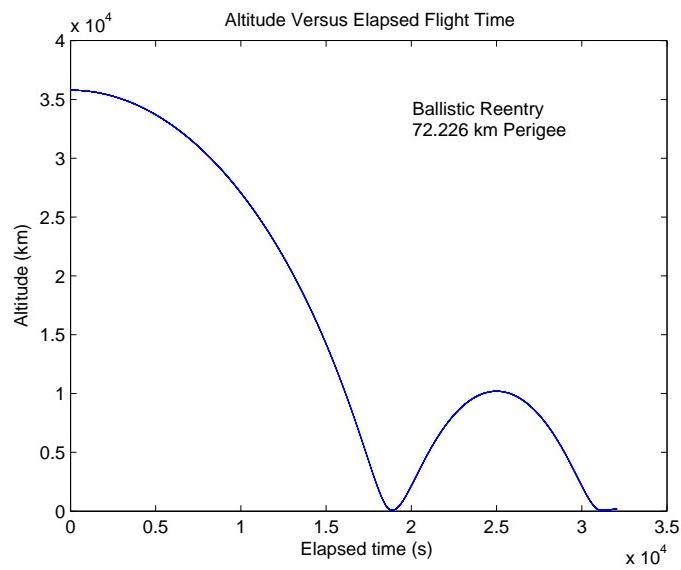
Figure 39:   SMV Altitude Versus Elapsed Time for Ballistic Reentry, 72.226 km Perigee
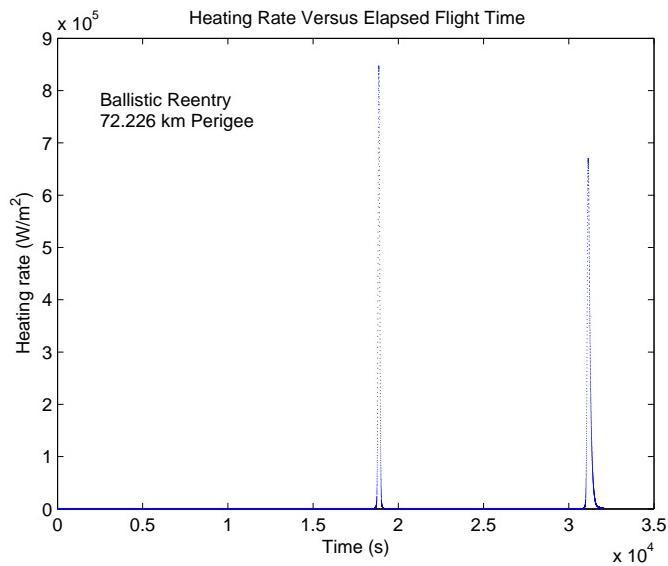
Figure 40:   SMV Heating Rate Versus Elapsed Time for Ballistic Reentry, 72.226 km Perigee
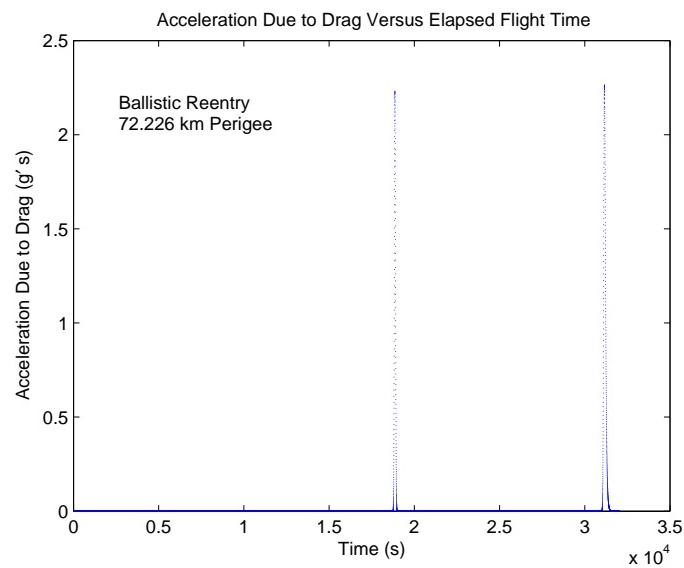
Figure 41:   Acceleration Due to Drag Versus Elapsed Time for Ballistic Reentry, 72.226 km Perigee
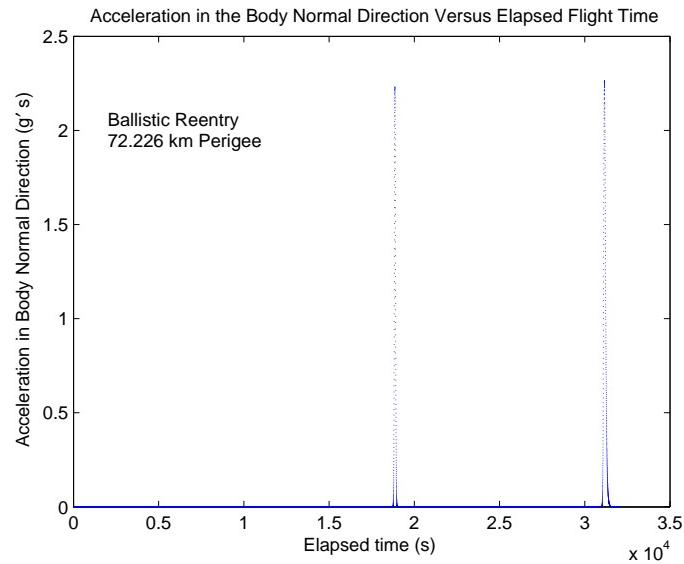
Figure 42:   Acceleration in Body Normal Direction Versus Elapsed Time for Ballistic Reentry, 72.226 km Perigee
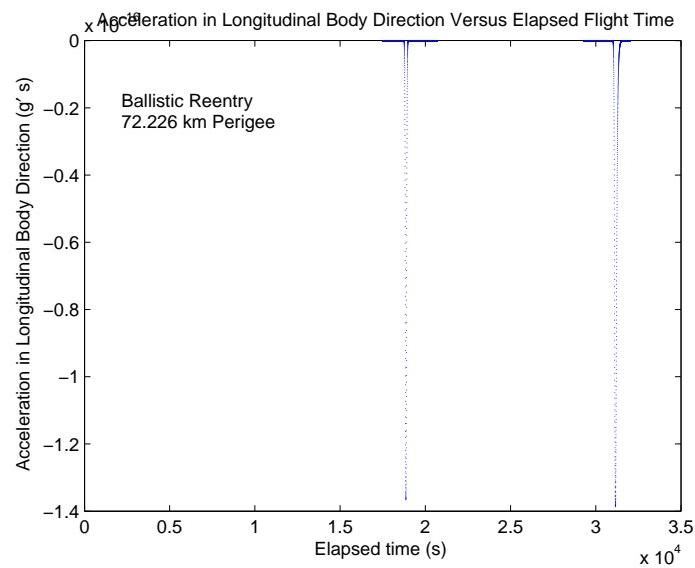
Figure 43:   Acceleration in Longitudinal Direction Versus Elapsed Time for Ballistic Reentry, 72.226 km Perigee
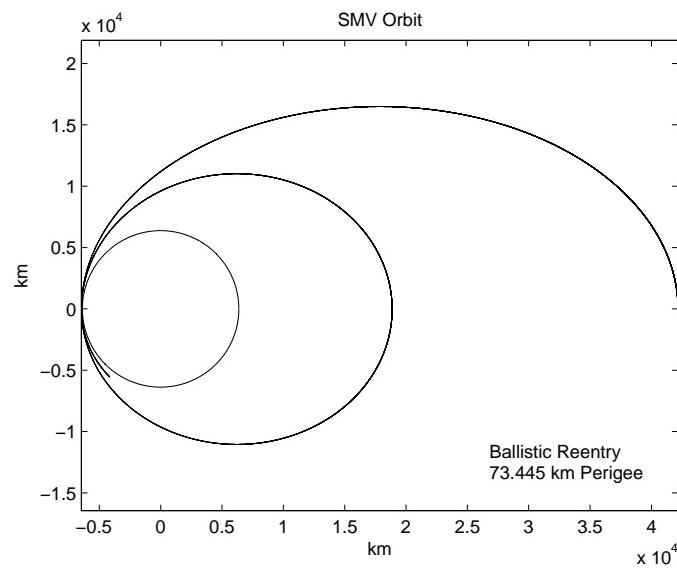
Figure 44:   Orbit for Ballistic Reentry, 73.445 km Perigee
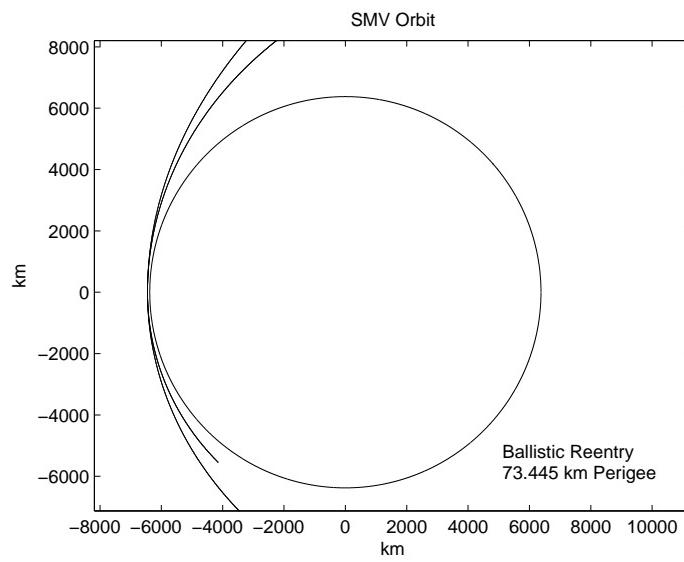
Figure 45:   Near Earth Portion of Orbit for Ballistic Reentry, 73.445 km Perigee
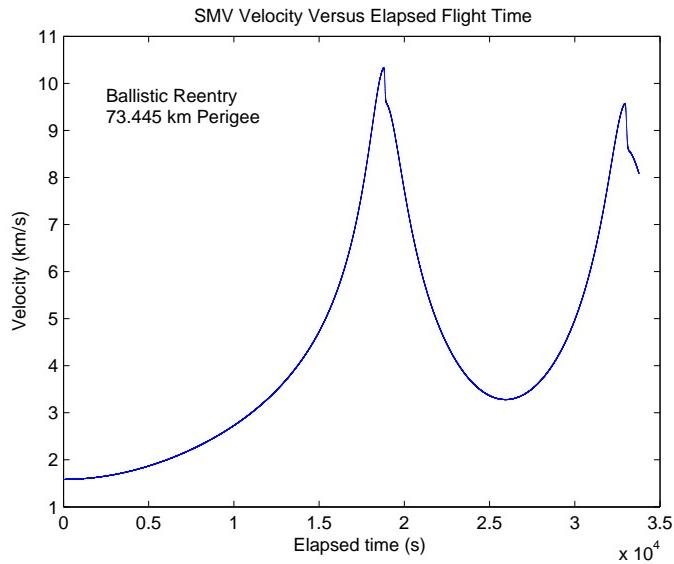
Figure 46: SMV Velocity Versus Elapsed Time for Ballistic Reentry, 73.445 km Perigee
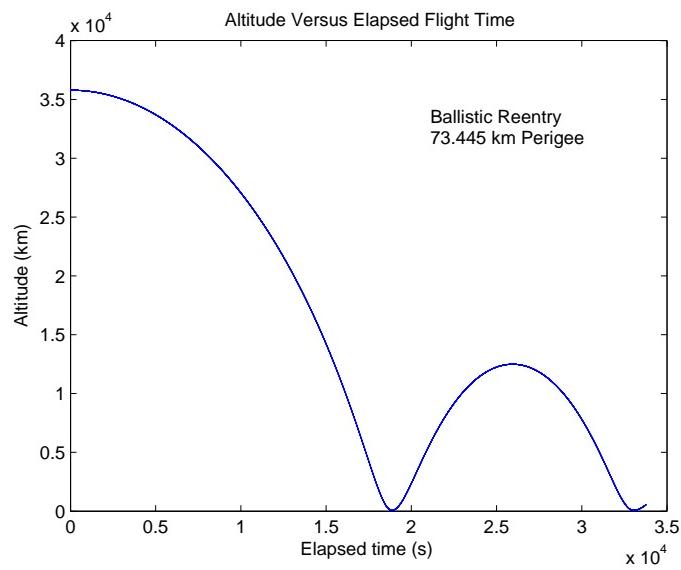
Figure 47: SMV Altitude Versus Elapsed Time for Ballistic Reentry, 73.445 km Perigee
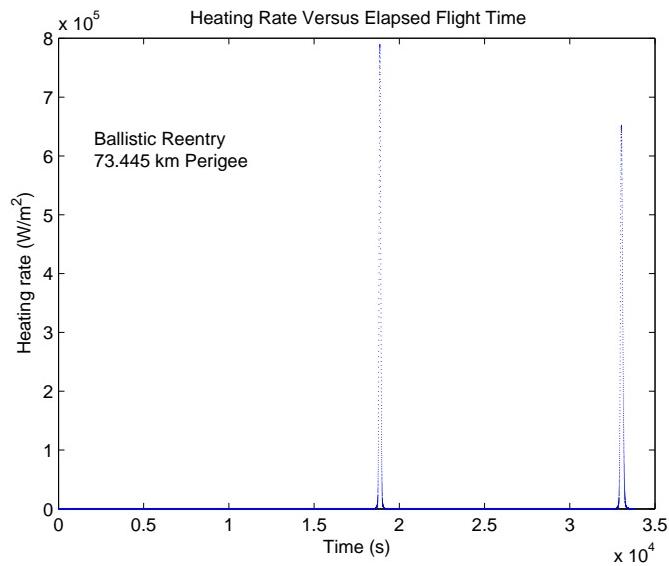
Figure 48:   SMV Heating Rate Versus Elapsed Time for Ballistic Reentry, 73.445 km Perigee
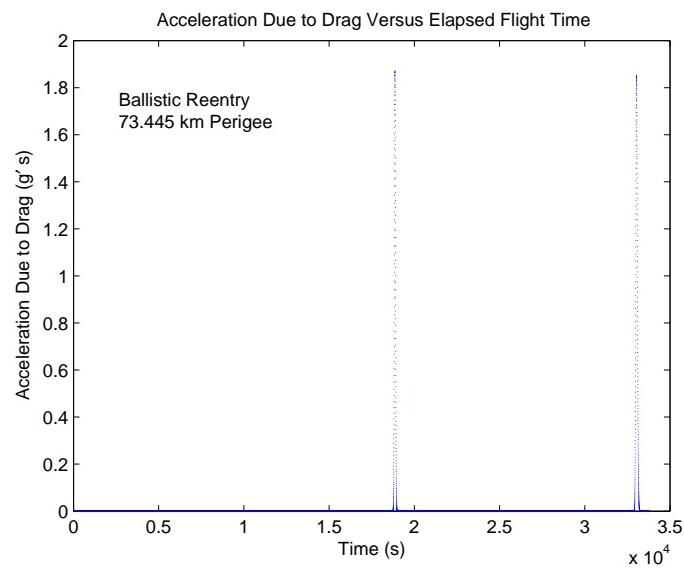
Figure 49:   Acceleration Due to Drag Versus Elapsed Time for Ballistic Reentry, 73.445 km Perigee

71
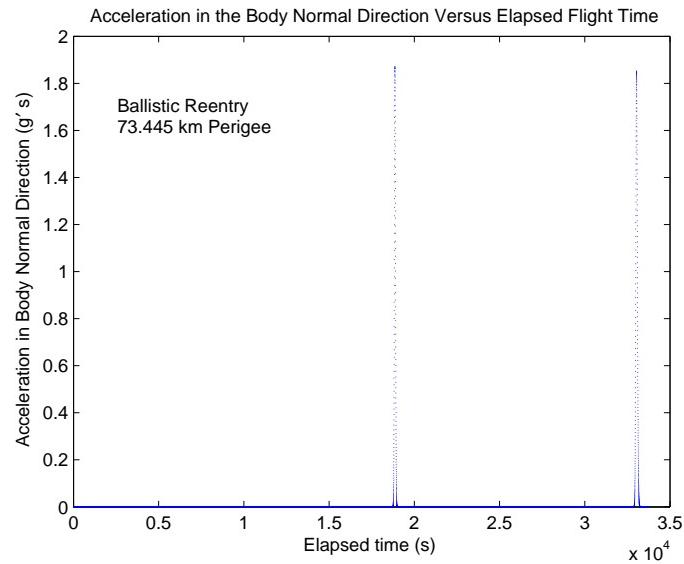
Figure 50: Acceleration in Body Normal Direction Versus Elapsed Time for Ballistic Reentry, 73.445 km Perigee
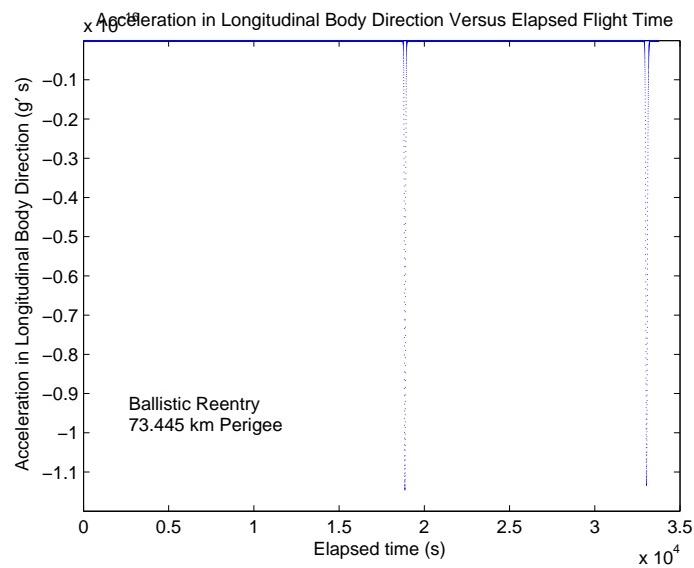
Figure 51: Acceleration in Longitudinal Direction Versus Elapsed Time for Ballistic Reentry, 73.445 km Perigee
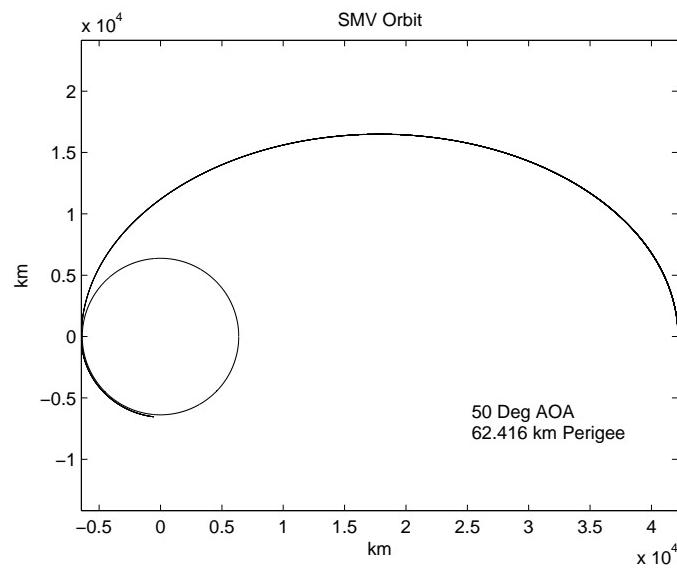
Figure 52:   Orbit for 50° AOA, 62.416 km Perigee
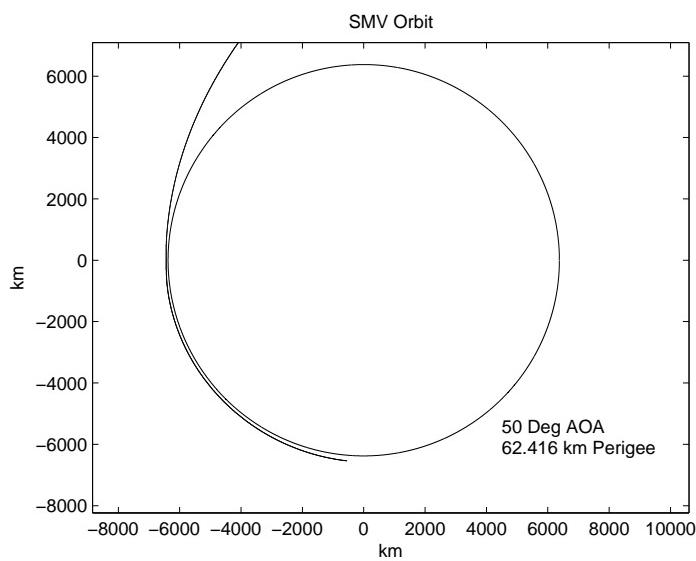
Figure 53:   Near Earth Portion of Orbit for 50° AOA, 62.416 km Perigee
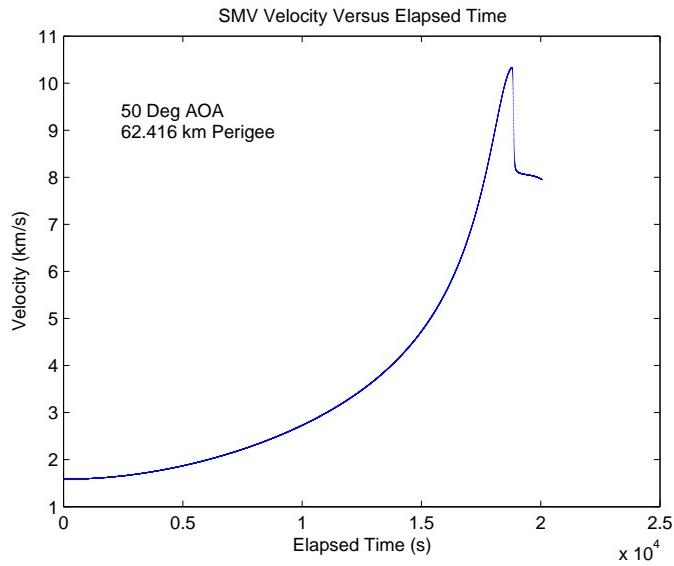
Figure 54:   SMV Velocity Versus Elapsed Time for 50° AOA, 62.416 km Perigee
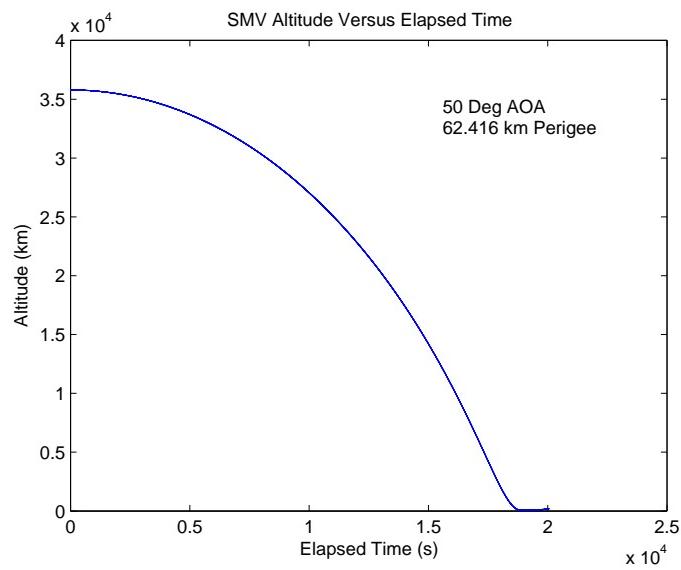
Figure 55:   SMV Altitude Versus Elapsed Time for 50° AOA, 62.416 km Perigee

74
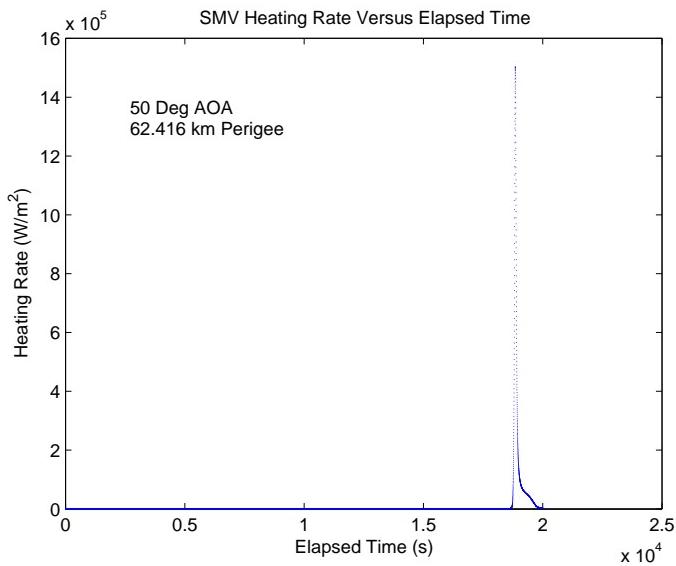
Figure 56:   SMV Heating Rate Versus Elapsed Time for 50° AOA, 62.416 km Perigee
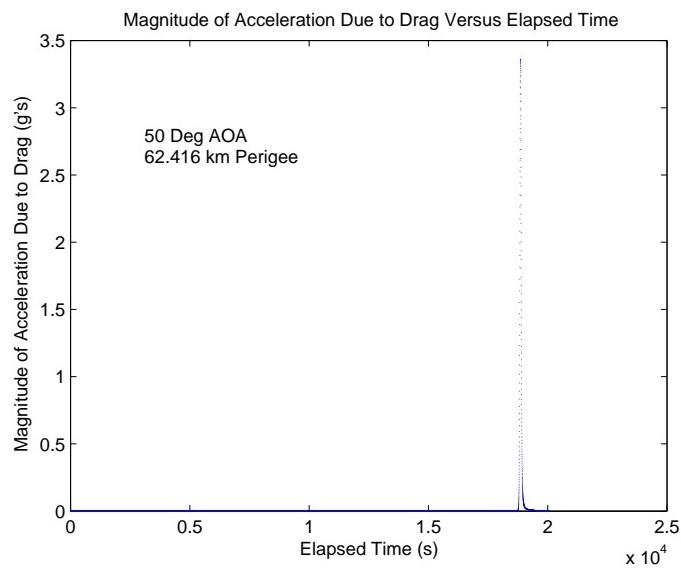
Figure 57:   Acceleration Due to Drag Versus Elapsed Time for 50° AOA, 62.416 km Perigee
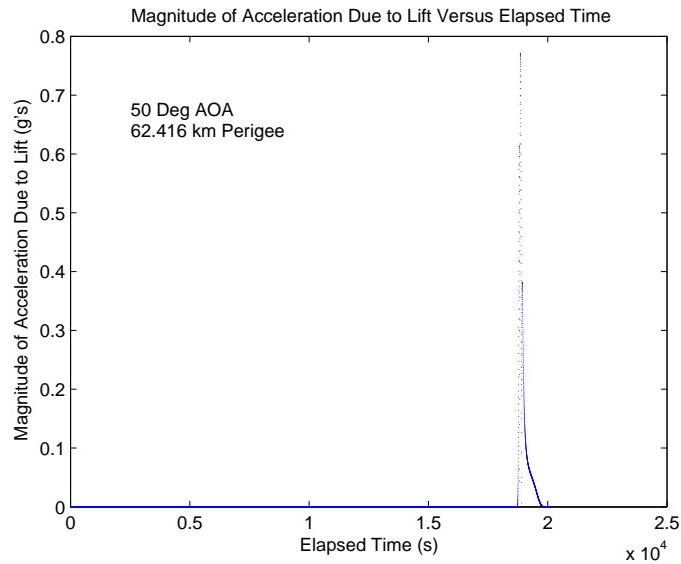
Figure 58:   Acceleration Due to Lift Versus Elapsed Time for 50° AOA, 62.416 km Perigee
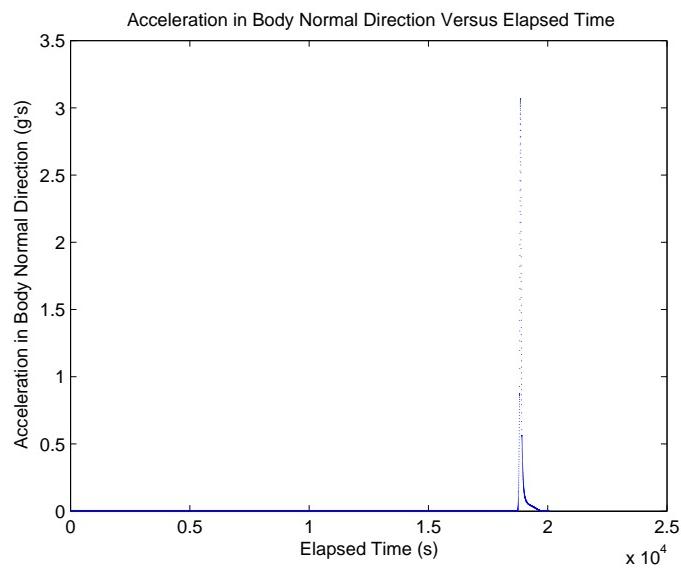
Figure 59:   Acceleration in Body Normal Direction Versus Elapsed Time for 50° AOA, 62.416 km Perigee
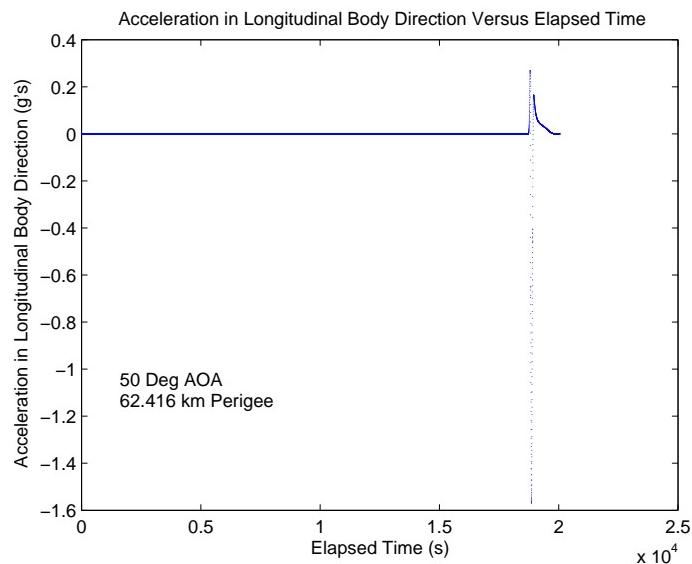
Figure 60:   Acceleration in Longitudinal Body Direction Versus Elapsed Time for 50° AOA, 62.416 km Perigee
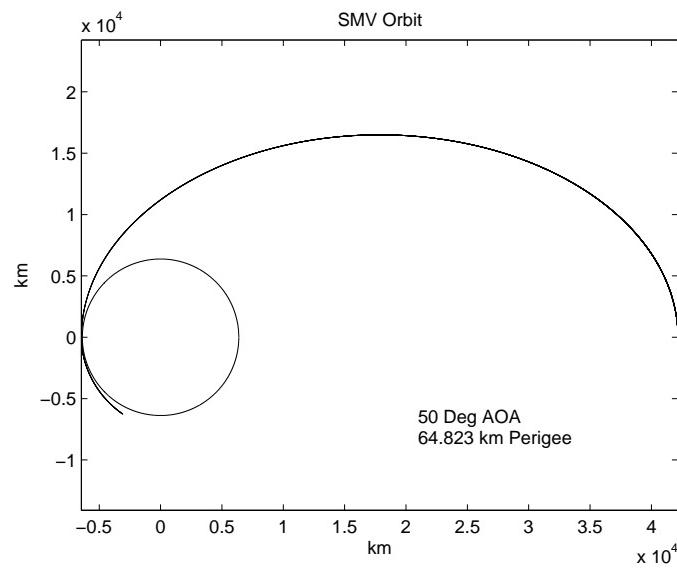
Figure 61:   Orbit for 50° AOA, 64.823 km Perigee
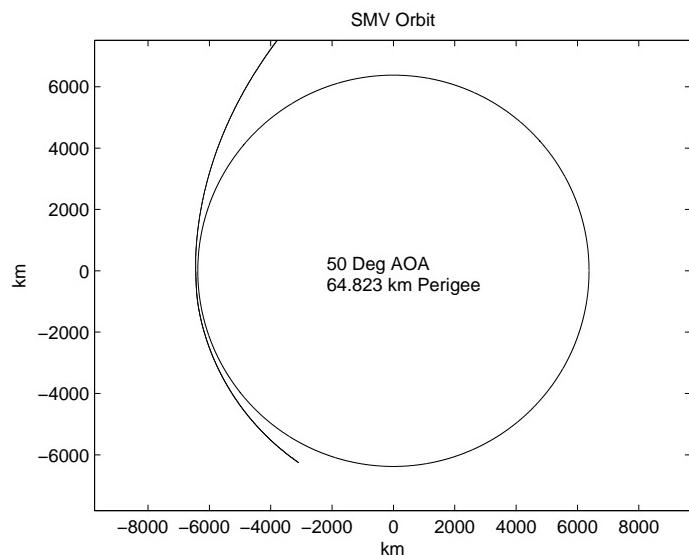
Figure 62:   Near Earth Portion of Orbit for 50° AOA, 64.823 km Perigee
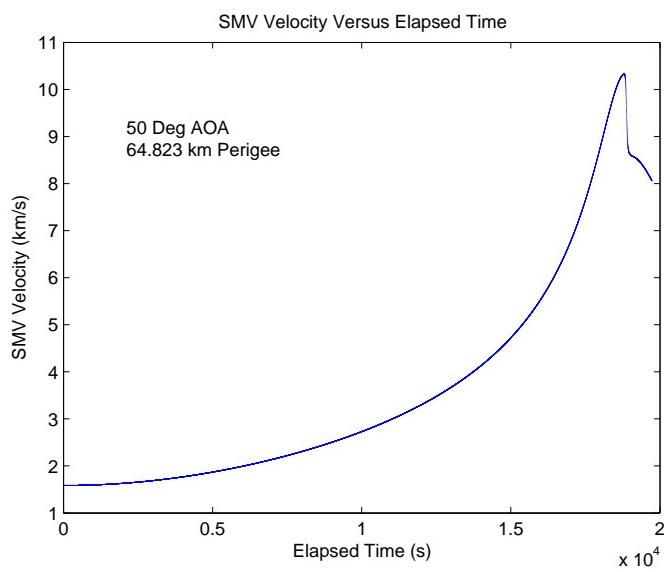

Figure 63:   SMV Velocity Versus Elapsed Time for 50° AOA, 64.823 km Perigee
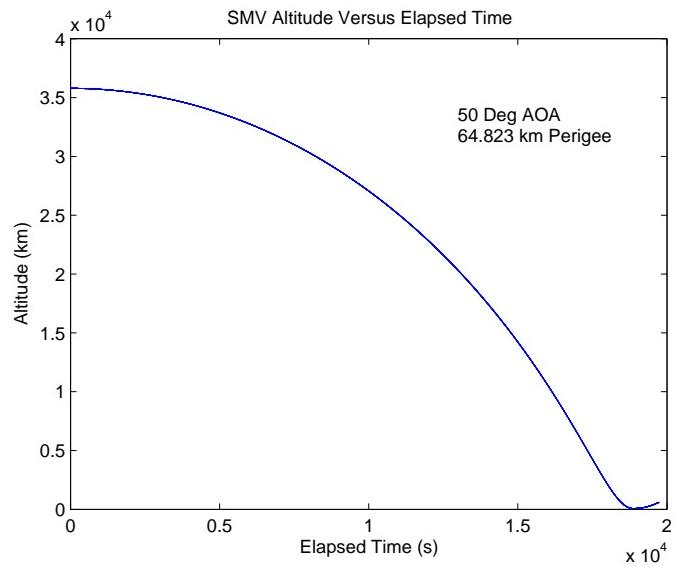
Figure 64:   SMV Altitude Versus Elapsed Time for 50° AOA, 64.823 km Perigee
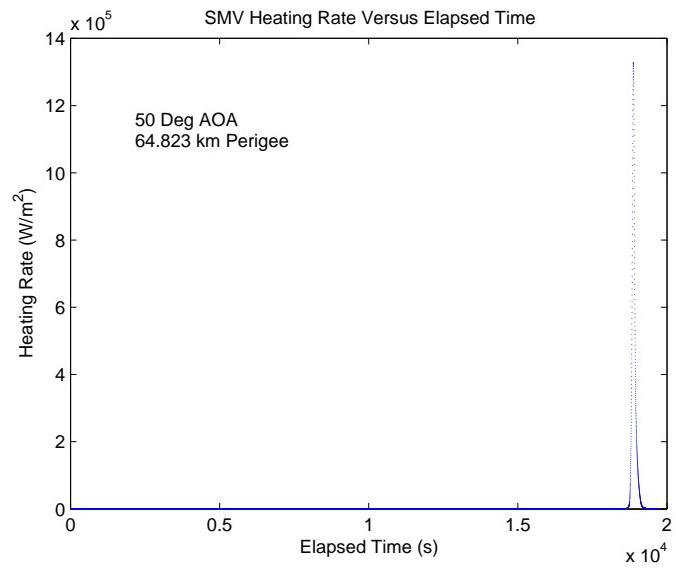

Figure 65:   SMV Heating Rate Versus Elapsed Time for 50° AOA, 64.823 km Perigee

79
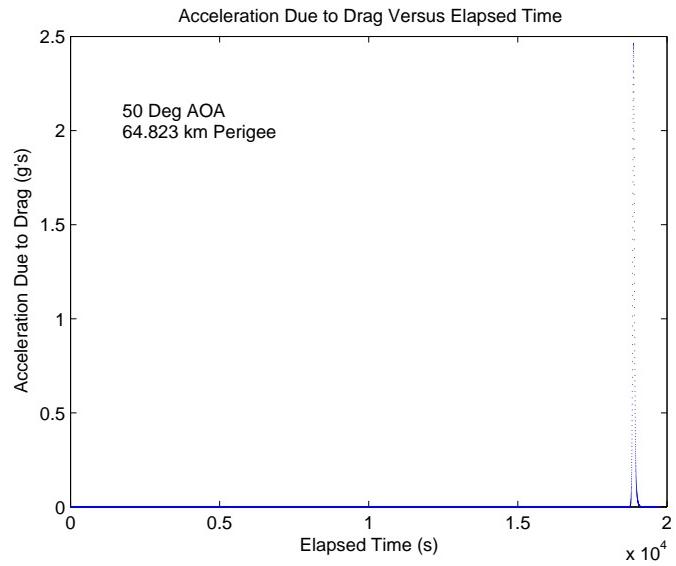
Figure 66: Acceleration Due to Drag Versus Elapsed Time for 50° AOA, 64.823 km Perigee
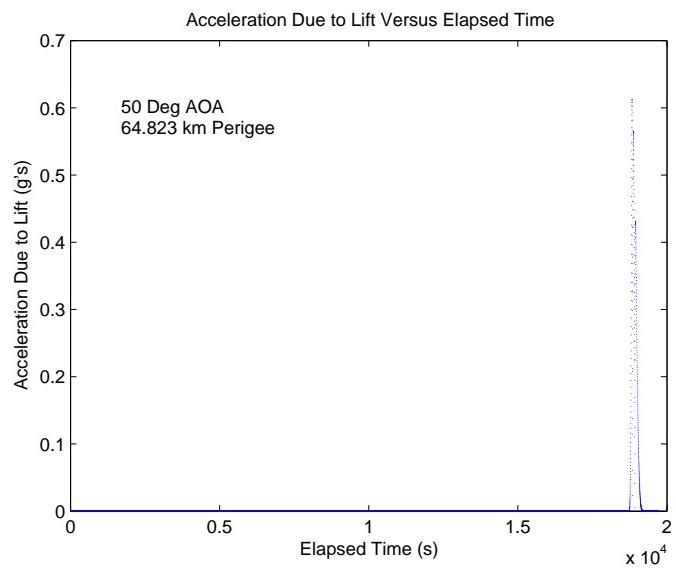

Figure 67: Acceleration Due to Lift Versus Elapsed Time for 50° AOA, 64.823 km Perigee
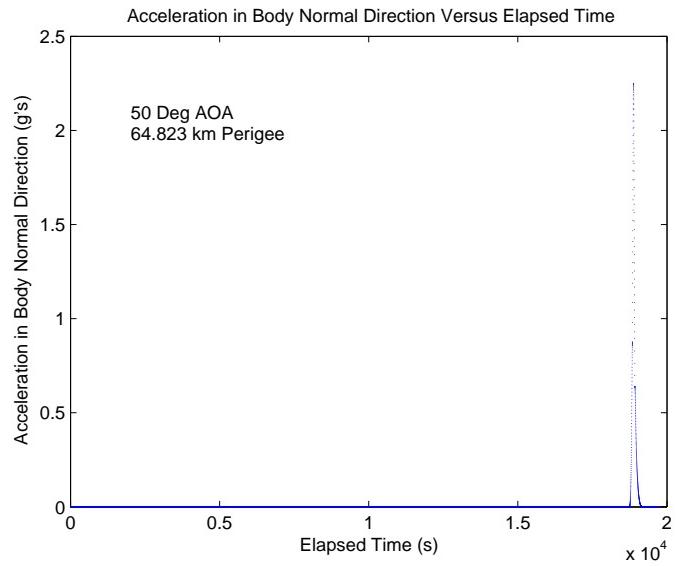
Figure 68:   Acceleration in Body Normal Direction Versus Elapsed Time for 50°
AOA, 64.823 km Perigee
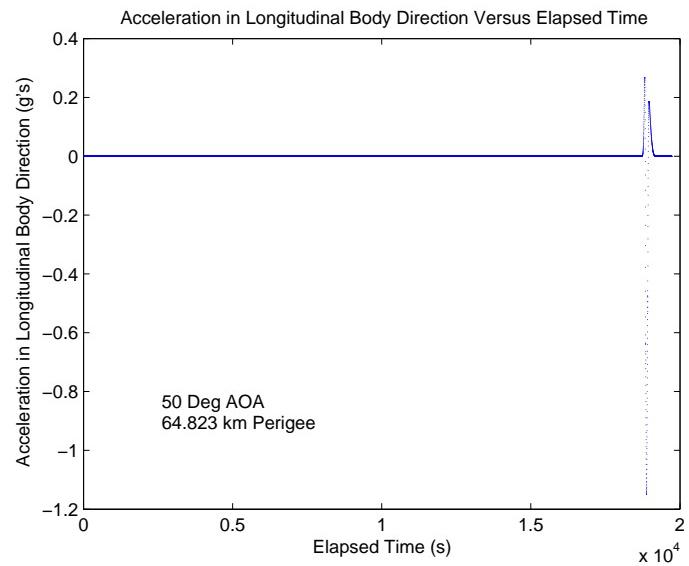
Figure 69:   Acceleration in Longitudinal Body Direction Versus Elapsed Time for
50° AOA, 64.823 km Perigee
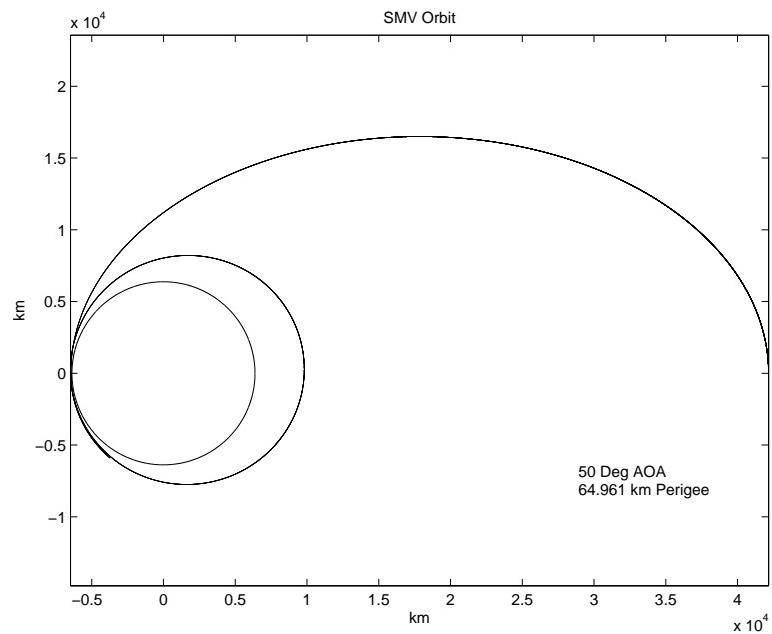
Figure 70:   Orbit for 50° AOA, 64.961 km Perigee
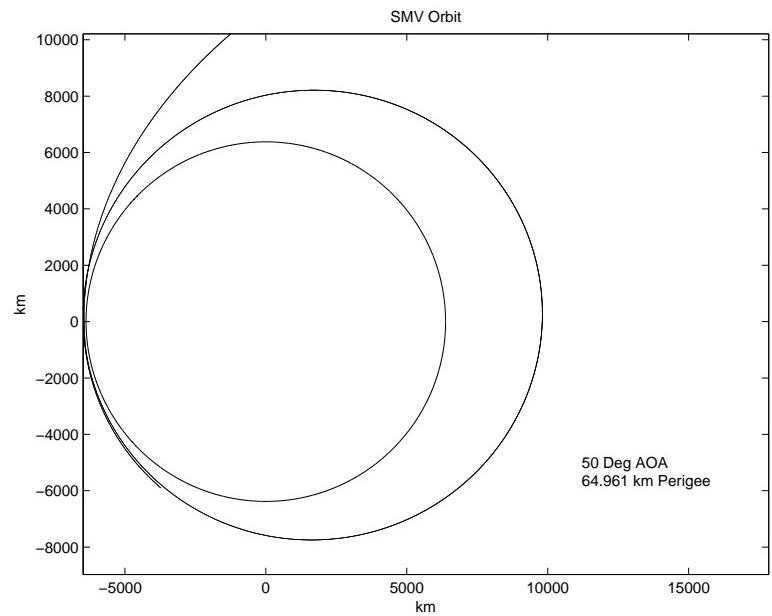
Figure 71:   Near Earth Portion of Orbit for 50° AOA, 64.961 km Perigee

82
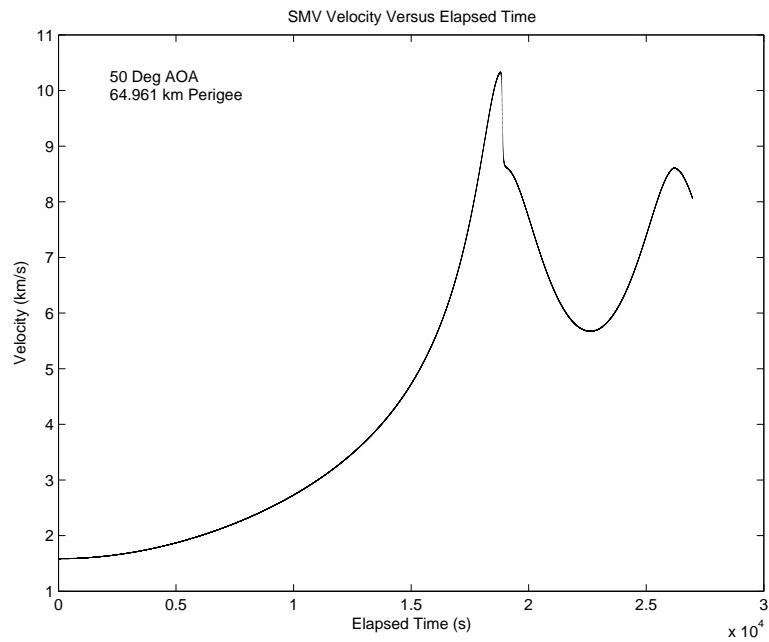
Figure 72:   SMV Velocity Versus Elapsed Time for 50° AOA, 64.961 km Perigee
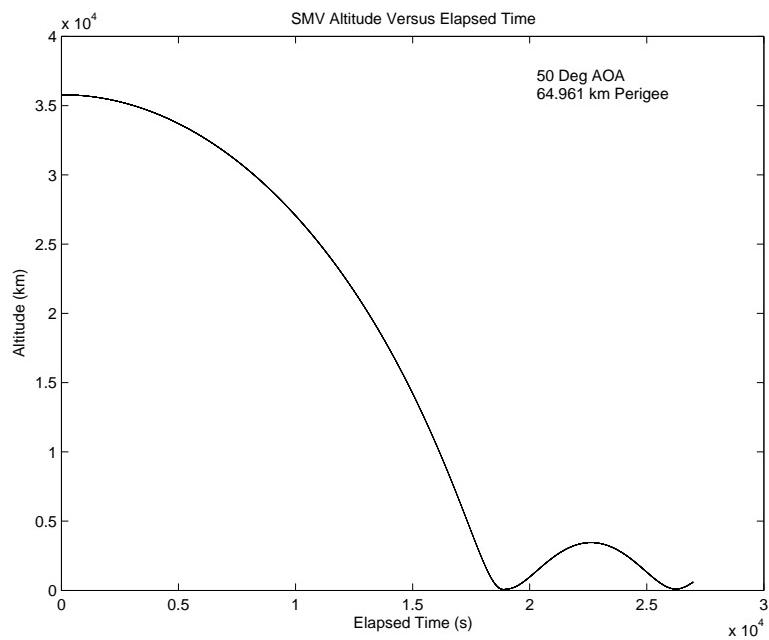
Figure 73:   SMV Altitude Versus Elapsed Time for 50° AOA, 64.961 km Perigee
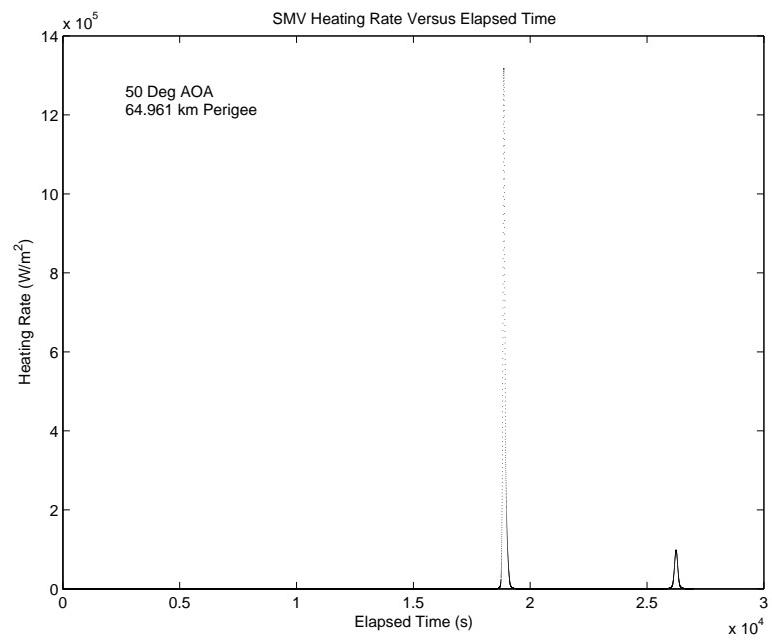
Figure 74:   SMV Heating Rate Versus Elapsed Time for 50° AOA, 64.961 km Perigee
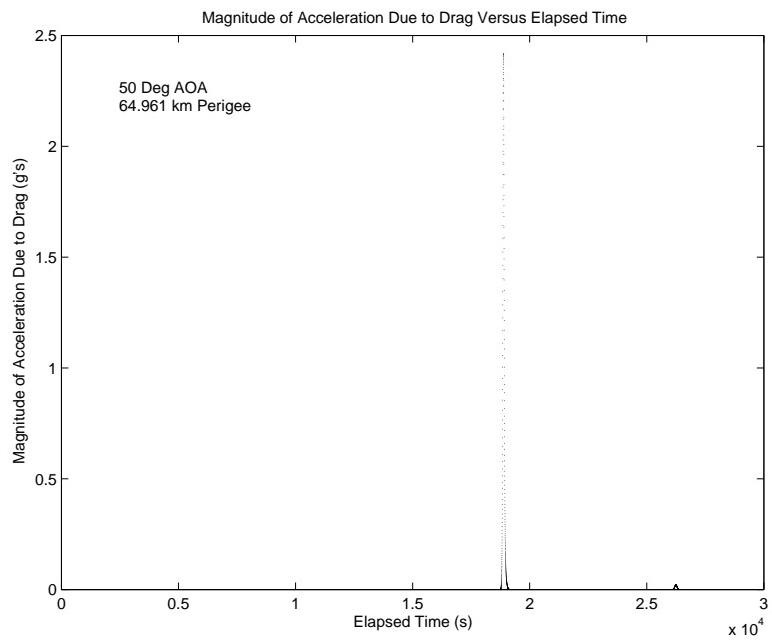
Figure 75:   Acceleration Due to Drag Versus Elapsed Time for 50° AOA, 64.961 km Perigee

84
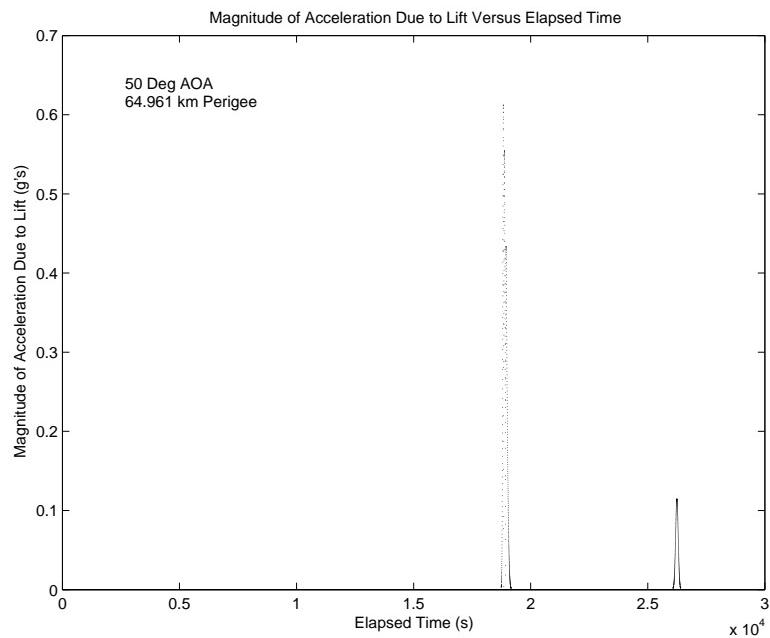
Figure 76:   Acceleration Due to Lift Versus Elapsed Time for 50° AOA, 64.961 km Perigee
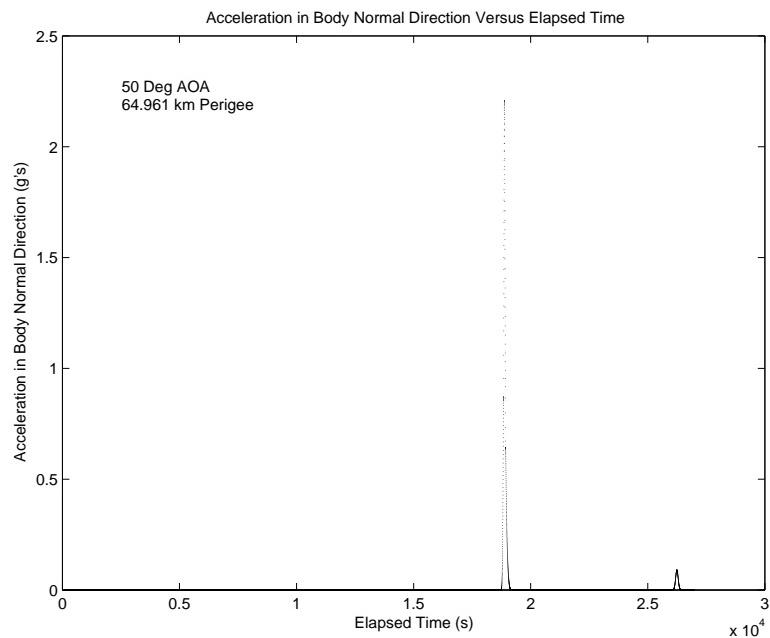
Figure 77:   Acceleration in Body Normal Direction Versus Elapsed Time for 50° AOA, 64.961 km Perigee
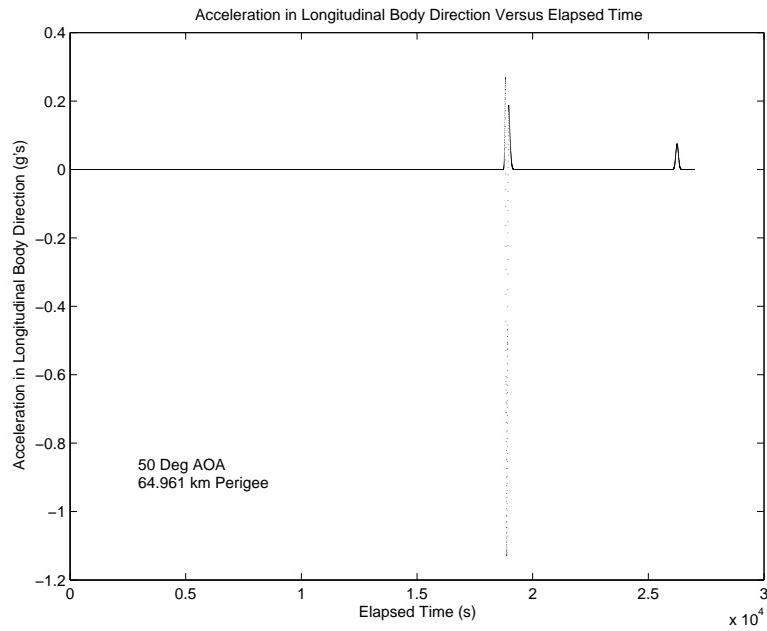
Figure 78: Acceleration in Longitudinal Body Direction Versus Elapsed Time for 50° AOA, 64.916 km Perigee
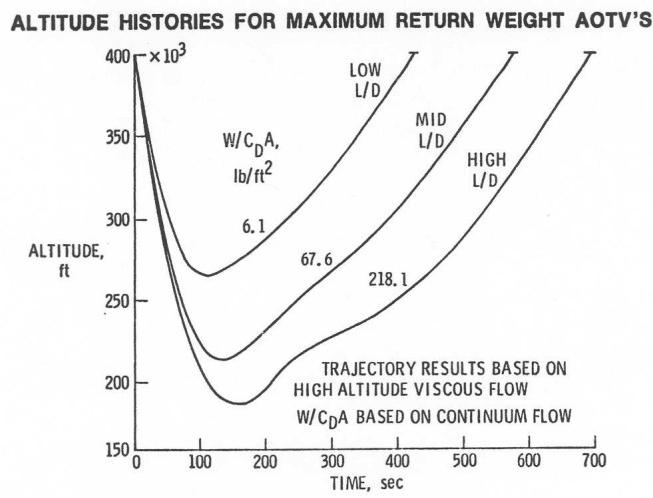
Figure 79: Altitude History for Maximum Return Weight AOTV [15, 47]
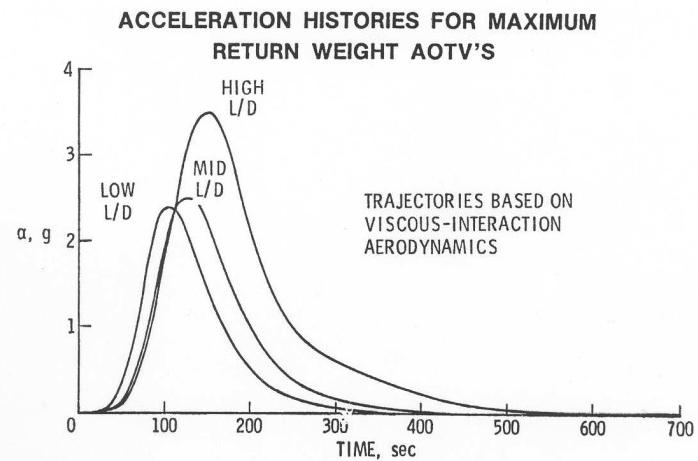
Figure 80:   Acceleration Histories for Maximum Return Weight AOTVs [15, 48]
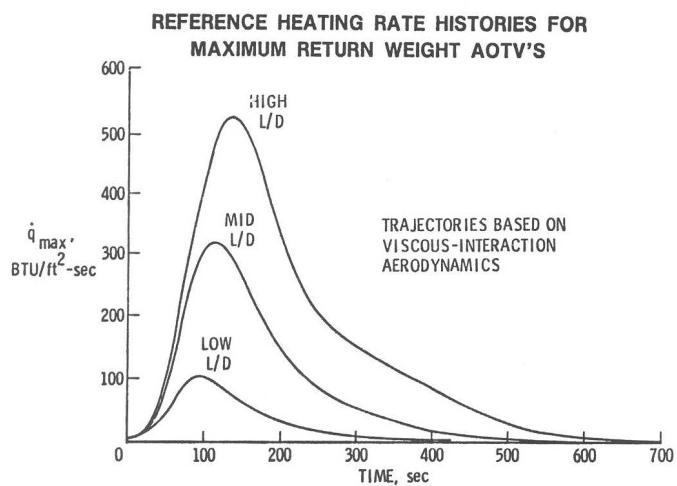
Figure 81:   Reference Heating Rate Histories for Maximum Return Weight AOTVs [15, 49]

87

Appendix B.

Measurements are scaled to the vehicle length: L = 29 ft (8.84m)

a. 0.174L

b. 0.279L

c. 0.220L

d. 0.152L

e. 0.175L
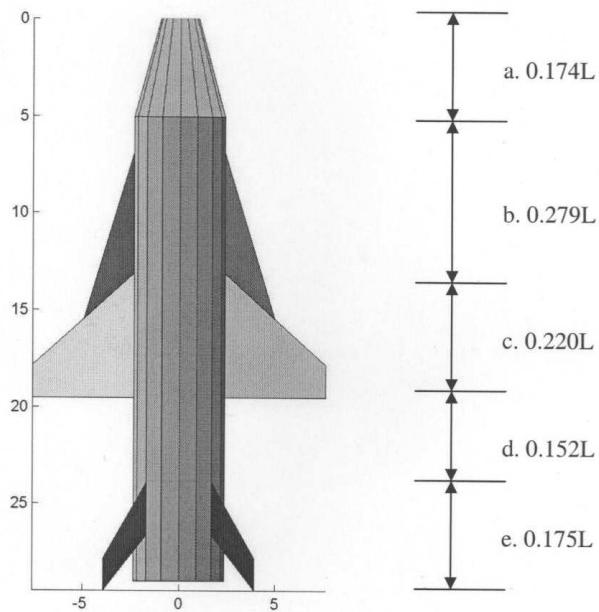
Figure 50: MATLAB SMV Model Top View 1

a. Nose Length
b. Length from Nose to forward lifting surface
c. Forward lifting surface inboard length
d. Length from rear of forward lifting surface to front of rear stabilizer
e. Length from front of rear stabilizer to rear of vehicle

Figure 82:   MATLAB SMV Model Top View [13, 73]

Measurements are scaled to the vehicle length: L = 29 ft (8.84m)
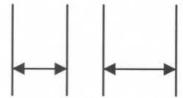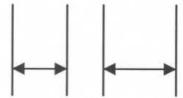
f. 0.058L g. 0.093L   h. 0.058L   i. 0.238L
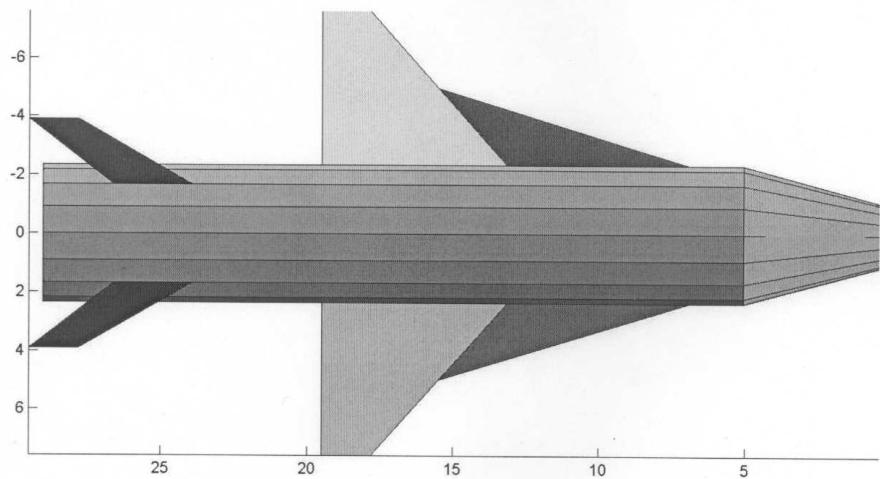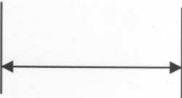
Figure 51: MATLAB SMV Model Top View 2

f. Rear stabilizer outboard length
g. Rear stabilizer inboard length
h. Forward lifting surface outboard length
i. Delta wing inboard length

Figure 83:   MATLAB SMV Model Top View 2 [13, 74]

Measurements are scaled to the vehicle length: L = 29 ft (8.84m)

j. θ = 45°

6   4   2   0   -2   -4   -6

k. 0.069L

l. 0.163L

m. 0.523L
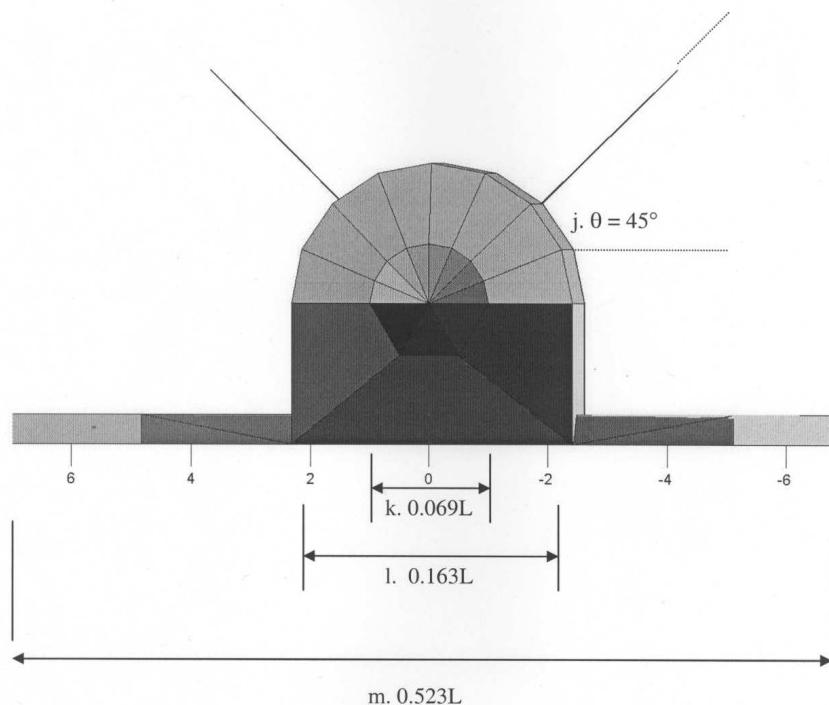
Figure 52: MATLAB SMV Model Front View

j.   Rotation angle for Rear Stabilizer
k.   Nose diameter
l.   Body width
m. Wingspan

Figure 84:   MATLAB SMV Model Front View [13, 75]

90

Appendix C.
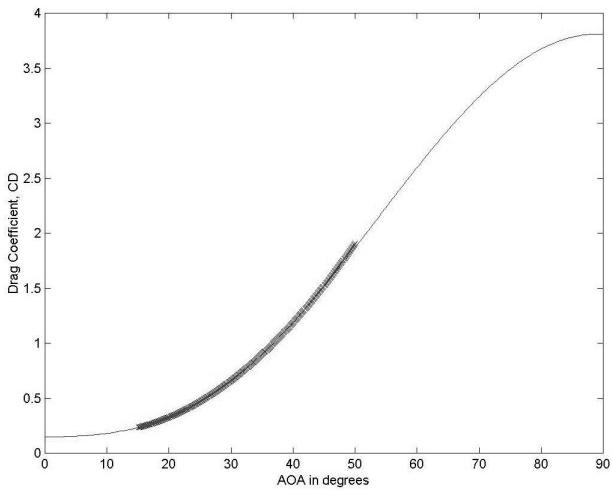
Figure 85:   Coefficient of Drag in Continuum vs Angle of Attack
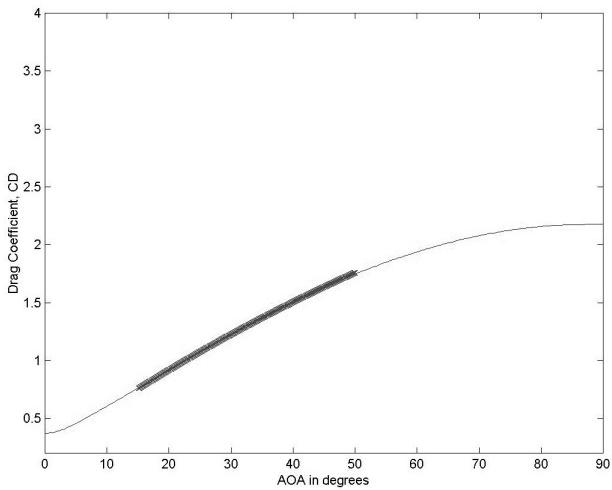
Figure 86:   Coefficient of Drag in Free Flow vs Angle of Attack

91
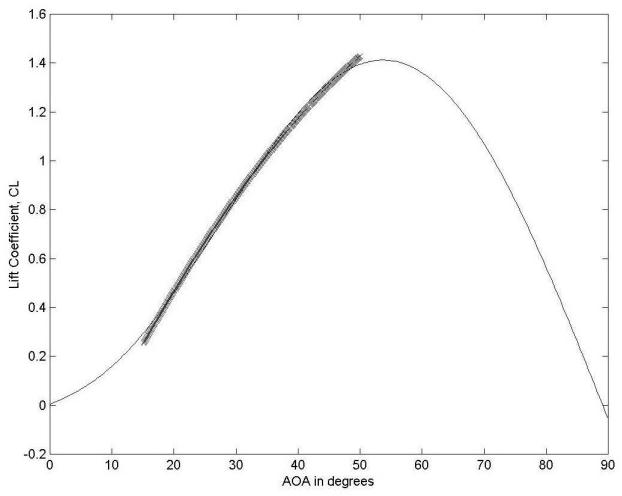
Figure 87:   Coefficient of Lift in Continuum vs Angle of Attack
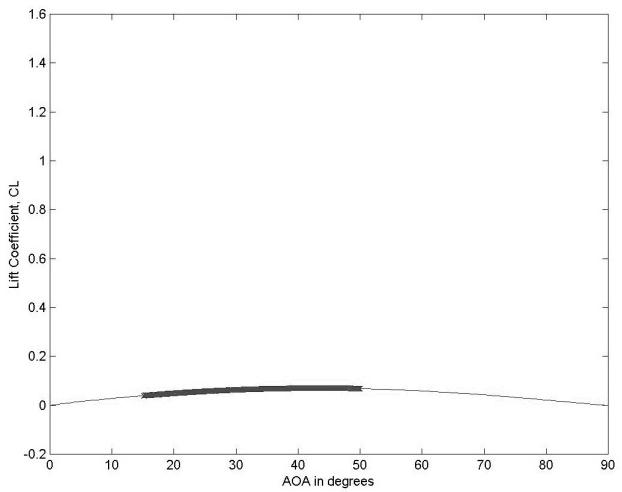
Figure 88:   Coefficient of Lift in Free Flow vs Angle of Attack

92

Table 17:   Lift and Drag Coefficients in Continuum

AOA in Deg	C_D	C_L	C_L / C_D
1	0.2261	-0.4485	-1.9831
2	0.2140	-0.3943	-1.8420
3	0.2038	-0.3407	-1.6713
4	0.1956	-0.2878	-1.4714
5	0.1893	-0.2356	-1.2446
6	0.1849	-0.1841	-0.9952
7	0.1825	-0.1332	-0.7297
8	0.1820	-0.0829	-0.4557
9	0.1834	-0.0333	-0.1819
10	0.1868	0.0155	0.0831
11	0.1920	0.0637	0.3320
12	0.1993	0.1113	0.5588
13	0.2084	0.1583	0.7594
14	0.2195	0.2045	0.9318
15	0.2325	0.2501	1.0758
16	0.2475	0.2951	1.1924
17	0.2643	0.3394	1.2838
18	0.2831	0.3830	1.3526
19	0.3039	0.4260	1.4016
20	0.3266	0.4683	1.4339
21	0.3512	0.5099	1.4520
22	0.3777	0.5509	1.4584
23	0.4062	0.5912	1.4555
24	0.4366	0.6309	1.4449
25	0.4689	0.6699	1.4285

Table 18:   Lift and Drag Coefficients in Continuum

AOA in Deg	C_D	C_L	C_L / C_D
26	0.5032	0.7082	1.4074
27	0.5394	0.7459	1.3828
28	0.5775	0.7829	1.3555
29	0.6176	0.8192	1.3265
30	0.6596	0.8549	1.2961
31	0.7035	0.8900	1.2650
32	0.7494	0.9243	1.2334
33	0.7971	0.9580	1.2018
34	0.8469	0.9911	1.1702
35	0.8985	1.0235	1.1390
36	0.9521	1.0552	1.1082
37	1.0076	1.0862	1.0780
38	1.0651	1.1166	1.0483
39	1.1245	1.1464	1.0194
40	1.1858	1.1754	0.9912
41	1.2490	1.2039	0.9638
42	1.3142	1.2316	0.9371
43	1.3813	1.2587	0.9112
44	1.4504	1.2851	0.8860
45	1.5213	1.3109	0.8616
46	1.5942	1.3360	0.8380
47	1.6691	1.3605	0.8150
48	1.7459	1.3842	0.7928
49	1.8246	1.4074	0.7713
50	1.9052	1.4298	0.7504

Table 19:   Lift and Drag Coefficients in Free Molecular Flow

AOA in Deg	C_D	C_L	C_L / C_D
1	0.2636	0.0010	0.0040
2	0.3005	0.0042	0.0141
3	0.3372	0.0073	0.0218
4	0.3735	0.0103	0.0278
5	0.4096	0.0133	0.0325
6	0.4455	0.0162	0.0364
7	0.4811	0.0190	0.0395
8	0.5164	0.0217	0.0421
9	0.5514	0.0244	0.0442
10	0.5862	0.0269	0.0460
11	0.6207	0.0294	0.0474
12	0.6550	0.0318	0.0486
13	0.6890	0.0342	0.0496
14	0.7227	0.0365	0.0505
15	0.7562	0.0386	0.0511
16	0.7894	0.0408	0.0516
17	0.8223	0.0428	0.0521
18	0.8549	0.0448	0.0524
19	0.8873	0.0466	0.0526
20	0.9195	0.0485	0.0527
21	0.9514	0.0502	0.0528
22	0.9830	0.0518	0.0527
23	1.0143	0.0534	0.0527
24	1.0454	0.0549	0.0525
25	1.0762	0.0563	0.0524

Table 20:   Lift and Drag Coefficients in Free Molecular Flow

AOA in Deg	C_D	C_L	C_L / C_D
26	1.1067	0.0577	0.0521
27	1.1370	0.0590	0.0519
28	1.1670	0.0602	0.0515
29	1.1968	0.0613	0.0512
30	1.2263	0.0623	0.0508
31	1.2556	0.0634	0.0505
32	1.2845	0.0642	0.0500
33	1.3132	0.0651	0.0495
34	1.3416	0.0658	0.0490
35	1.3698	0.0665	0.0485
36	1.3977	0.0670	0.0480
37	1.4253	0.0675	0.0474
38	1.4527	0.0680	0.0468
39	1.4798	0.0683	0.0462
40	1.5066	0.0686	0.0455
41	1.5332	0.0688	0.0449
42	1.5595	0.0689	0.0442
43	1.5856	0.0690	0.0435
44	1.6114	0.0690	0.0428
45	1.6369	0.0689	0.0421
46	1.6621	0.0687	0.0413
47	1.6871	0.0684	0.0406
48	1.7118	0.0681	0.0398
49	1.7363	0.0677	0.0390
50	1.7605	0.0672	0.0382

Bibliography

1.   Air Force Research Laboratory Space Vehicles Directorate (AFRL/SV). "Space Maneuver Vehicle." n.pag. http://www.vs.afrl.af.mil/Factsheets/smv.html 15 December 2004.

2.   Bate, Roger R. and others. *Fundamentals of Astrodynamics*. New York: Dover Publications, Inc., 1971.

3.   Cohen, William. "Department of Defense Space Policy Memorandum." http://www.au.af.mil/au.awc/awcgate/dod-spc/dodspcpolicy99.pdf 26 October 2005.

4.   David, Leonard. "NASA Shuts Down X-33, X-44." n.pag. http://www.space.com/missionlaunches/ 26 October 2004.

5.   Dryden Flight Research Center. "X-37 Approach and Landing Test Vehicle (ALTV)." n.pag. http://www.nasa.gov/centers/Dryden/news/ResearchUpdate/X-37/index.html 26 October 2004.

6.   -----. "X-40A Project Update." n.pag. http://www.dfrc.nasa.gov/Research/X40A/ 26 October 2004.

7.   Federation of American Scientists. "X-33 VentureStar." n.pag. http://www.fas.org/spp/guide/usa/launch/x-33.htm 26 October 2004.

8.   -----. "X-34." n.pag. http://www.fas.org/spp/guide/usa/launch/x-34 26 October 2004.

9.   Hicks, Kerry D. Class handout, MECH 637, Astrodynamic Reentry. Department of Aeronautics and Astronautics, Air Force Institute of Technology, Wright-Patterson AFB OH, Winter 2005.

10.   Kilgore, Tim R. *Mini-spaceplane (Space Maneuver Vehicle) Operational Utility*. Technical Report, Seal Beach, California: Boeing Company, 1997.

11.   Kreyszig, Erwin. *Advanced Engineering Mathematics* (2nd Edition). New York: John Wiley and Sons, Inc., 1999.

12.   Lu, Ping. "Entry Guidance and Trajectory Control for Reusable Launch Vehicle," *Journal of Guidance, Control, and Dynamics*, 20:143-149 (January-February 1997).

13. McNabb, Dennis J. *Investigation of Atmospheric Reentry for the Space Maneuver Vehicle*. MS thesis, AFIT/GA/ENY/04-M03, School of Engineering and Management, Air Force Institute of Technology (AU), 2004.

14. Moster, Greg. "Reusable Military Launch System Team," *AFRL Technology Horizon*, 38-40 (April 2004).

15. National Aeronautics and Space Administration. *Performance Assessment of Aero-assisted Orbital Transfer Vehicles*. Technical Report N85-16993. Hampton, Virginia: National Aeronautics and Space Administration, 1985.

16. -----. "Illustration of the X-37 Advanced Technology Demonstrator During Flight." n.pag. http://www.dfrc.nasa.gov/Gallery/Photo/X-37/HTML/EC99-45145-2.html 27 October 2004.

17. -----. "NASA to Roll Out X-34 Technology Demonstrator April 30 at Dryden Flight Research Center." n.pag. http://www1.msfc.nasa.gov/NEWSROOM/news/releases/1999/99-068.html 26 October 2004.

18. -----. "X-33 Advanced Technology Demonstrator." n.pag. http://www1.msfc.nasa.gov/NEWSROOM/background/facts/x33.html 26 October 2004.

19. National Aeronautics and Space Administration/ Kennedy Space Center Information Technology Directorate. "NSTS 1988 News Reference Manual." n.pag. http://science.ksc.nasa.gov/shuttle/technology/sts-newsref/stsref-toc.html 15 January 2005.

20. Regan, Frank J. and Satya Anandakrishnan. *Dynamics of Atmospheric Re-Entry*. Washington, DC: American Institute of Aeronautics and Astronautics, Inc., 1993.

21. Space.com. "NASA, Boeing to Develop and Fly X-37." n.pag. http://www.space.com/businesstechnology/business/x37.html 27 October 2004.

22. Vallado, David A. *Fundamentals of Astrodynamics and Applications* (2nd Edition). El Segundo: Microcosm Press, 2001.

23. Wiesel, William. *Spaceflight Dynamics* (2nd Edition). Boston: The McGraw-Hill Companies, Inc., 1997.

Vita

Benjamin Marc Berlin graduated from Centennial High School in Franklin, Tennessee. He then attended the United States Air Force Academy in Colorado Springs, Colorado. He was commissioned as a second lieutenant on 28 May 2003. Immediately after graduation from the United States Air Force Academy he was assigned to the Air Force Institute of Technology where he earned the degree of Master of Science in Astronautical Engineering in March 2005. Upon graduation, he was was assigned to Detachment 12, Space and Missile Systems Center, Kirtland Air Force Base.

1. Type of Product: Compact Disc	2. Operating System/Version: Windows/XP	3. New Product or Replacement: New Product	4. Type of File: Matlab .m files Text file
5. Language/Utility Program: Matlab and Notepad			
6. # of Files/# of Products: 14 m files 1 text file	**7. Character Set:**	**8. Disk Capacity:**	
	9. Compatibility:	**10. Disk Size:**	

11. Title: AFIT/GA/ENY/05-M01

12. Performing Organization: AFIT/ENY	13. Performing Report #: AFIT/GA/ENY/05-M01	14. Contract #:
		15. Program Element #:
16. Sponsor/Monitor: Dr. William Wiesel Dr. Harry Karasopoulos	17. Sponsor/Monitor # Acronym: AFIT/ENY	19. Project #:
	18. Sponsor/Monitor #:	20. Task #:
		21. Work Unit #:

22. Date: 21 March 2005	23. Classification of Product: U
24. Security Classification Authority: Unclassified	25. Declassification/Downgrade Schedule:

26. Distribution/Availability: Approved for public release; Distribution Unlimited

DTIC FORM 530 JUN 94	Security Classification of this Page:

27. Abstract:

28. Classification of Abstract:

29. Limitation of Abstract:

30. Subject Terms:

30a. Classification of Subject Terms:

31. Required Peripherals:

32. # of Physical Records:

33. # of Logical Records:

34. # of Tracks:

35. Record Type:

36. Color:

37. Recording System:

38. Recording Density:

39. Parity:

40. Playtime:

41. Playback Speed:

42. Video:

43. Text:

44. Still Photos:

45. Audio:

46. Other:

47. Documentation/Supplemental Information:

48. Point of Contact and Telephone Number:

Benjamin Berlin, 255-3636

					Form Approved

REPORT DOCUMENTATION PAGE

Form Approved
OMB No. 074-0188

1. REPORT DATE *(DD-MM-YYYY)*	**2. REPORT TYPE**	**3. DATES COVERED** *(From – To)*
21-03-2005	**Master's Thesis**	April 2004 – March 2005

4.   TITLE AND SUBTITLE

Investigation of Aerobraking to Return the Space Maneuver Vehicle to Low Earth Orbit from Geotransfer Orbit

5a. CONTRACT NUMBER

5b. GRANT NUMBER

5c. PROGRAM ELEMENT NUMBER

6.   AUTHOR(S)

Berlin, Benjamin, M., Second Lieutenant, USAF

5d. PROJECT NUMBER

5e. TASK NUMBER

5f. WORK UNIT NUMBER

7. PERFORMING ORGANIZATION NAMES(S) AND ADDRESS(S)
   Air Force Institute of Technology
   Graduate School of Engineering and Management (AFIT/EN)
   2950 Hobson Way
   WPAFB OH 45433-7765

8. PERFORMING ORGANIZATION REPORT NUMBER

AFIT/GA/ENY/05-M01

9. SPONSORING/MONITORING AGENCY NAME(S) AND ADDRESS(ES)
   HQ AFSPC/DRX
   Attn: Dr. Harry Karasopoulos
   Peterson AFB, 80914   DSN: 692-4405

10. SPONSOR/MONITOR'S ACRONYM(S)

11. SPONSOR/MONITOR'S REPORT NUMBER(S)

12. DISTRIBUTION/AVAILABILITY STATEMENT
      APPROVED FOR PUBLIC RELEASE; DISTRIBUTION UNLIMITED.

13. SUPPLEMENTARY NOTES

14. ABSTRACT
This study investigated the use of ballistic and ``Double-Dip'' aerobraking reentry to return the Space Maneuver Vehicle (SMV) from geotransfer orbit in no more than two atmosphere passes. Lift and drag accelerations were applied to the two-body problem when either of their magnitudes exceeded 1/1000 g. Lift and drag coefficients, along with the SMV model, were taken from *Investigation of Atmospheric Reentry for the Space Maneuver Vehicle* by Captain McNabb, AFIT/GA/ENY/04-M03. Target perigees were formulated using the two-body problem. The orbit from each target perigee was numerically integrated around a planar earth model using a fourth order Runge-Kutta method. Ballistic and ``Double-Dip'' reentry schemes were attempted with 45 and 70 km altitude floors. Ballistic reentry produced a near circular, low earth orbit when the SMV's true perigee altitude resided between 66.801 and 68.449 km for a one pass reentry and between 72.226 and 73.445 km for a two pass reentry. ``Double-Dip'' reentry produced a near circular, low earth orbit when the SMV's perigee altitude rested between 62.416 and 64.962 km. The resulting perigee windows, their respective heating rates, and experienced accelerations were analyzed. Effects of uncertainty in the atmosphere model on successful perigee windows for each reentry scheme were analyzed by repeating the simulation with an increased atmospheric density.

15. SUBJECT TERMS
Reentry Vehicle, Atmosphere Entry, Space Maneuver Vehicle, Reentry Aerodynamics

16. SECURITY CLASSIFICATION OF:			**17. LIMITATION OF ABSTRACT**	**18. NUMBER OF PAGES**	**19a. NAME OF RESPONSIBLE PERSON** William Wiesel, Civ, USAF (ENY)
REPORT U	**ABSTRACT** U	**c. THIS PAGE** U	**UU**	116	**19b. TELEPHONE NUMBER** *(Include area code)* (937) 255-6565, ext 4312; e-mail: William.Wiesel@afit.edu

Standard Form 298 (Rev: 8-98)
Prescribed by ANSI Std. Z39-18